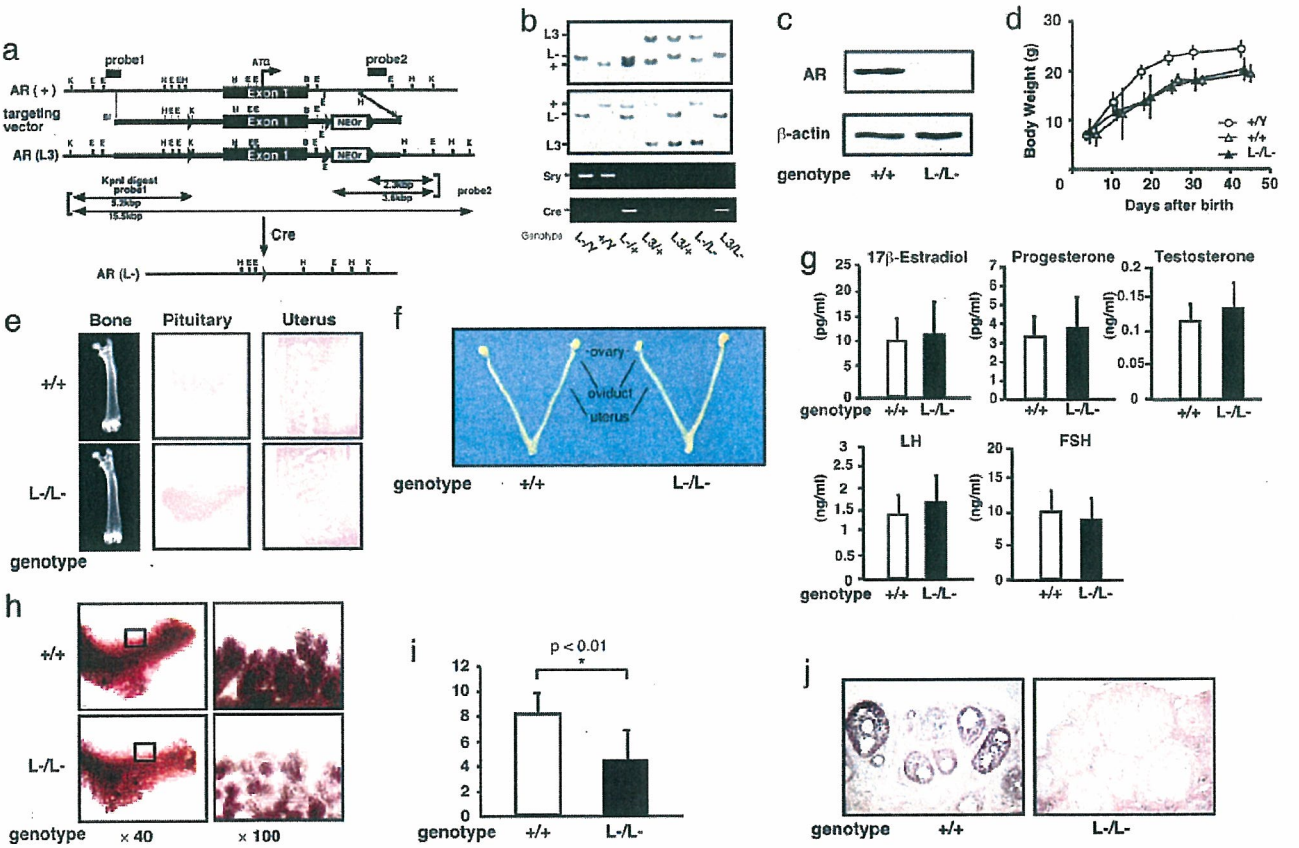

Fig. 1. Phenotypic characterization of AR knockout female mice. (*a*) Diagram of the wild-type *Ar* genomic locus (+), floxed *AR* L3 allele (L3), and *AR* allele (L-) obtained after Cre-mediated excision of exon 1. K, KpnI; E, EcoRI; H, HindIII; B, BamHI. LoxP sites are indicated by arrowheads. The targeting vector consisted of a 7.6-kb 5′ homologous region containing exon 1, a 1.3-kb 3′ homologous region, a single loxP site, and the neo cassette with two loxP sites. (*b*) Detection of the Y chromosome-specific *Sry* gene in $AR^{-/Y}$ mice by PCR. (*c*) Absence of AR protein in $AR^{-/-}$ mice ovaries by Western blot analysis using a specific C-terminal antibody. (*d*) Normal weight gain in $AR^{-/-}$ females. (*e*) Histology of pituitary, uterus, and bone tissues in $AR^{+/+}$ and $AR^{-/-}$ females at 8 weeks of age. (*f*) Female reproductive organs were macroscopically normal in $AR^{-/-}$ mice. (*g*) Serum hormone levels at the proestrus stage in $AR^{-/-}$ mice were not significantly altered. Serum 17β-estradiol, progesterone, testosterone, luteinizing hormone (LH), and follicle-stimulating hormone (FSH) levels in $AR^{+/+}$ ($n = 13$) and $AR^{-/-}$ ($n = 10$) females at 8–10 weeks of age are shown. (*h*) Lobuloalveolar development is impaired in $AR^{-/-}$ mammary glands. Whole mount of inguinal mammary glands (*Left*) and its higher magnification (*Right*) were prepared on day 3 of lactation. (*i*) Average number of pups per litter is markedly reduced in $AR^{-/-}$ mice at 8 weeks of age. Data are shown as mean ± SEM and analyzed by using Student's *t* test. (*j*) AR immunocytochemistry in $AR^{+/+}$ and $AR^{-/-}$ ovaries. Sections were counterstained with eosin.

more layers of granulosa cells with no antrum), or antral follicles (antrum within the granulosa cell layers enclosing the oocyte). Follicles were determined to be atretic if they displayed two or more of the following criteria within a single cross section: more than two pyknotic nuclei, granulosa cells within the antral cavity, granulosa cells pulling away from the basement membrane, or uneven granulosa cell layers (15).

Immunohistochemistry. Sections were subjected to a microwave antigen retrieval technique by boiling in 10 mM citrate buffer (pH 6.0) in a microwave oven for 30 min (16). The cooled sections were incubated in 1% H_2O_2 for 30 min to quench endogenous peroxidase and then incubated with 1% Triton X-100 in PBS for 10 min. To block nonspecific antibody binding, sections were incubated in normal goat serum for 1 h at 4°C. Sections were then incubated with anti-AR (1:100) or anti-cleaved caspase-3 (1:100) in 3% BSA overnight at 4°C. Negative controls were incubated in 3% BSA without primary antibody. The ABC method was used to visualize signals according to the manufacturer's instructions. Sections were incubated in biotinylated goat anti-rabbit IgG (1:200 dilution) for 2 h at room temperature, washed with PBS, and incubated in avidin–biotin–horseradish peroxidase for 1 h. After thorough washing in PBS, sections were developed with 3,3′-diaminobendizine tetrahydrochloride substrate, slightly counterstained with eosin, dehydrated through an ethanol series and xylene, and mounted.

Estrus Cycles and Fertility Test. To determine the stage of the estrus cycle (proestrus, estrus, and diestrus), vaginal smears were taken every morning and stained with Giemsa solution. For evaluation of female fertility for 15 weeks, an 8- or 24-week-old wild-type or $AR^{-/-}$ female was mated with a wild-type fertile male, replaced every 2 weeks with the other fertile male. Cages were monitored daily and for an additional 23 days, and the presence of seminal plugs and number of litters were recorded.

RNA Extraction and Quantitative Competitive RT-PCR. Total ovarian RNA was extracted by using TRIzol (Invitrogen) (16). Oligo-dT-primed cDNA was synthesized from 1 μg of ovarian RNA by using SuperScript reverse transcriptase (Gibco BRL, Gaithersburg, MD) in a 20-μl reaction volume, 1 μl of which was then diluted serially (2- to 128-fold) and used to PCR-amplify an internal control gene, *cycA*, to allow concentration estimation.

PHYSIOLOGY

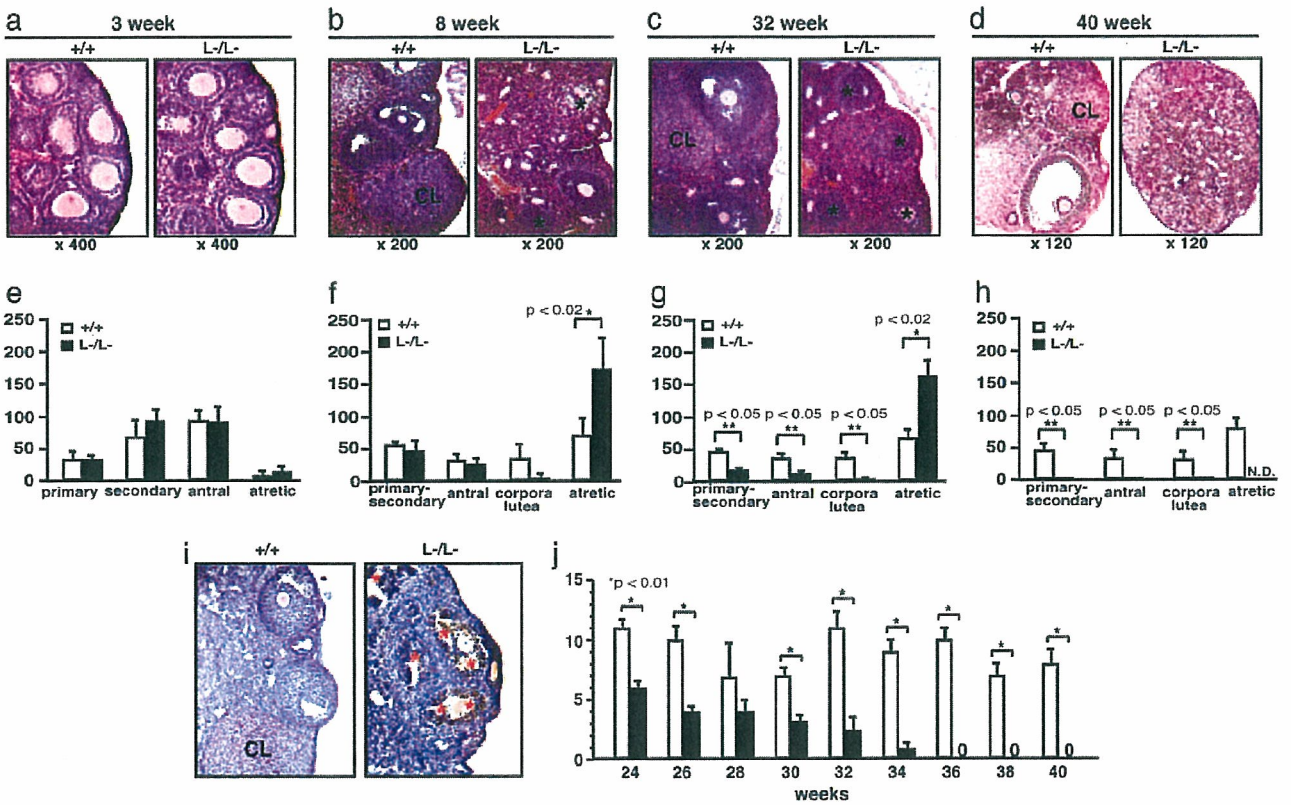

Fig. 2. POF in $AR^{-/-}$ female mice. (*a–d*) Histology of $AR^{+/+}$ and $AR^{-/-}$ ovaries at 3 weeks, 8 weeks, 32 weeks, and 40 weeks of age. All sections were stained with hematoxylin and eosin. An asterisk marks the atretic follicle. CL, corpus luteum. (*e–h*) Relative follicle counts at 3 weeks (*e*), 8 weeks (*f*), 32 weeks (*g*), and 40 weeks (*h*) of age. Numbers represent total counts of every fifth section from serially sectioned ovaries ($n = 4$ animals per genotype). (*i*) Immunohistochemical study for activated, cleaved caspase-3 revealed increased positive cells (apoptotic cells) in $AR^{-/-}$ ovaries. Sections were counterstained with hematoxylin. An asterisk marks the caspase-3-positive cell. CL, corpus luteum. (*j*) Age-dependent reduction in the number of pups per litter in $AR^{-/-}$ female mice. A continuous breeding assay was started at 24 weeks of age ($n = 6–10$ animals per genotype). For all panels, data are shown as mean ± SEM and were analyzed by using Student's *t* test.

Primers were designed from cDNA sequences of *Kitl* (M57647; nucleotides 1099–1751), Gdf9 (NM008110; nucleotides 720-1532), *Bmp15* (NM009757; nucleotides 146–973), *Ers2* (NM010157; nucleotides 1139–1921), *Pgr* (NM008829; nucleotides 1587–2425), *Cyp11a1* (NM019779; nucleotides 761-1697), *Cyp17al* (M64863; nucleotides 522–932), *Cyp19* (D00659; nucleotides 699-1049), *Fshr* (AF095642; nucleotides 625-1427), *Lhr* (M81310; nucleotides 592-1331), *Ptgs2* (AF338730; nucleotides 3–605), and *Ccnd2* (NM009829; nucleotides 150-1065) and chosen from different exons to avoid amplification from genomic DNA.

GeneChip Analysis. Ovaries were isolated and stabilized in RNA-*later* RNA Stabilization Reagent (Ambion, Austin, TX) before RNA purification (17). Total RNA was purified by using an RNeasy mini kit (Qiagen, Valencia, CA) according to the manufacturer's instructions. First-strand cDNA was synthesized from 5 μg of RNA by using 200 units of SuperScript II reverse transcriptase (Invitrogen, Carlsbad, CA), 100 pmol T7-$(dT)_{24}$ primer [5′-GGCCAGTGAATTGTAATACGACTCAC-TATAGGGAGGCGG-$(dT)_{24}$-3′], 1× first-strand buffer, and 0.5 mM dNTPs at 42°C for 1 h. Second-strand synthesis was performed by incubating first-strand cDNA with 10 units of *Escherichia coli* ligase (Invitrogen), 40 units of DNA polymerase I (Invitrogen), 2 units of RNase H (Invitrogen), 1× reaction buffer, and 0.2 mM dNTPs at 16°C for 2 h, followed by 10 units of T4 DNA polymerase (Invitrogen) and incubation for another 5 min at 16°C. Double-stranded cDNA was purified by using GeneChip Sample Cleanup Module (Affymetrix, Santa Clara, CA) according to the manufacturer's instructions and labeled by *in vitro* transcription by using a BioArray HighYield RNA transcript labeling kit (Enzo Diagnostics, Farmingdale, NY). Briefly, dsDNA was mixed with 1× HY reaction buffer, 1× biotin-labeled ribonucleotides (NTPs with Bio-UTP and Bio-CTP), 1× DTT, 1× RNase inhibitor mix, and 1× T7 RNA polymerase and incubated at 37°C for 4 h. Labeled cRNA was then purified by using GeneChip Sample Cleanup Module and fragmented in 1× fragmentation buffer at 94°C for 35 min. For hybridization to the GeneChip Mouse Expression Array 430A or 430B or Mouse Genome 430 2.0 Array (Affymetrix), 15 μg of fragmented cRNA probe was incubated with 50 pM control oligonucleotide B2, 1× eukaryotic hybridization control, 0.1 mg/ml herring sperm DNA, 0.5 mg/ml acetylated BSA, and 1× hybridization buffer in a 45°C rotisserie oven for 16 h. Washing and staining were performed by using a GeneChip Fluidic Station (Affymetrix) according to the manufacturer's protocol. Phycoerythrin-stained arrays were scanned as digital image files and analyzed with GENECHIP OPERATING SOFTWARE (Affymetrix) (17).

Luciferase Assay. The *Kitl* promoter region (−2866 to −1 bp) was inserted into the pGL3-basic vector (Promega) for assay using the Luciferase Assay System (Promega) (14, 16). Cells at 40–50% confluence were transfected with a reference pRL-CMV

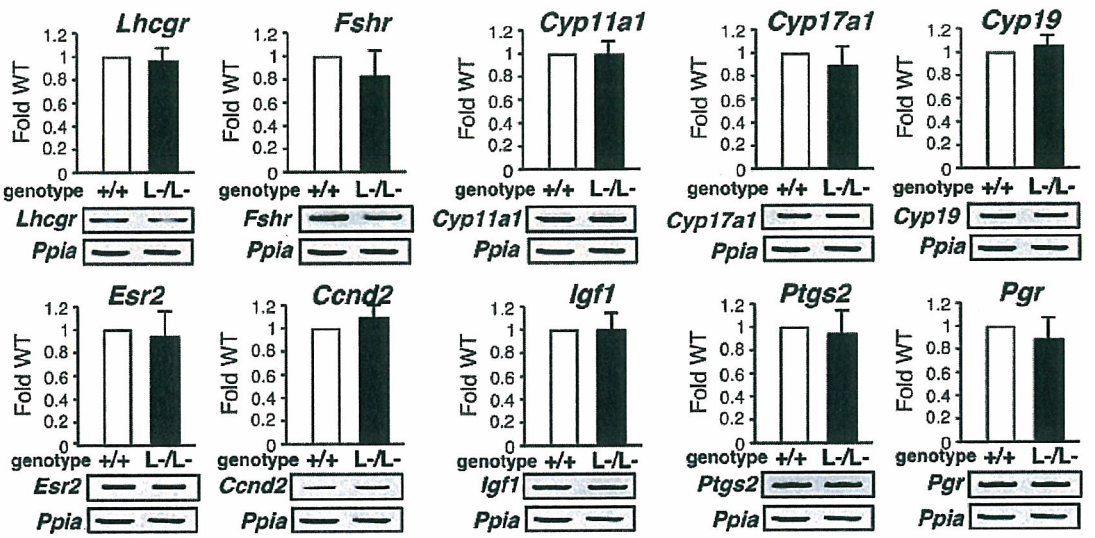

Fig. 3. No significant alterations in mRNA levels of several major regulators in folliculogenesis. Shown is semiquantitative RT-PCR of LH receptor (*Lhr*), FSH receptor (*Fshr*), p450 side chain cleavage enzyme (*Cyp11a1*), 17-α-hydroxylase (*Cyp17a1*), Aromatase (*Cyp19*), estrogen receptor-β (*Esr2*), cyclin D2 (*Ccnd2*), insulin-like growth factor 1 (*Igf1*), cyclooxygenase 2 (*Ptgs2*), or progesterone receptor (*Pgr*) gene expression in $AR^{+/+}$ and $AR^{-/-}$ ovaries. Results shown were representative (using one ovary per genotype in each experiment) of five independent experiments.

plasmid (Promega) using Lipofectamine reagent (GIBCO/BRL, Grand Island, NY) to normalize transfection. Results shown are representative of five independent experiments.

Results and Discussion

Subfertility of $AR^{-/-}$ Female Mice at 8 Weeks of Age. The *Ar* gene located on the X chromosome was disrupted in mice by using the Cre/Lox P system (6) (Fig. 1 *a–c*). Female $AR^{-/-}$ mice showed normal growth compared with the wild-type littermates (Fig. 1*d*), with no detectable bone loss (Fig. 1*e*) or obesity common for male $AR^{-/Y}$ mice (8, 9). Young (8-week-old) $AR^{-/-}$ females appeared indistinguishable from the wild-type littermates, displayed normal sexual behavior (7), and produced the first offspring of normal body size at the expected age. Macroscopic appearance of their reproductive organs, including uteri, oviducts, and ovaries, also appeared normal (Fig. 1*f*). Histological analysis showed no significant abnormality in the uterus or pituitary (Fig. 1*e*), whereas mammary ductal branching and elongation were substantially reduced, as revealed by whole-mount analysis (Fig. 1*h*). Serum levels of 17β-estradiol, progesterone, testosterone, luteinizing hormone, and follicle-stimulating hormone were also within normal range in 8-week-old mutant females at the proestrus stage (Fig. 1*g*), suggesting that the two-cell two-gonadotrophin system in female reproductive and endocrine organs (18) was intact in $AR^{-/-}$ mice at 8 weeks of age. The most obvious early sign of abnormal reproductive function in the $AR^{-/-}$ females was that their average numbers of pups per litter were only about half of those of the wild-type littermates, ($AR^{+/+}$, 8.3 ± 0.4 pups per litter; $AR^{-/-}$, 4.5 ± 0.5 pups per litter) (Fig. 1*i*).

$AR^{-/-}$ Female Mice Developed POF Phenotypes. Histological analysis of 8-week-old $AR^{-/-}$ ovaries clearly showed that numbers of atretic follicles were significantly increased, with decreased numbers of corpora lutea (Fig. 2 *b* and *f*). This finding suggests that the reduced pup numbers were due to impaired folliculogenesis in AR-deficient ovaries. Indeed, AR protein expression was readily detectable in the wild-type 8-week-old ovaries (Fig. 1*j*), with AR expressed at the highest levels in growing follicle granulosa cells at all developmental stages and at relatively low levels in corpora lutea. Thus, AR appears to play a regulatory role in granulosa cells during their maturation to the luteal phase.

To investigate this possibility, we examined the ovarian phenotype of female $AR^{-/-}$ mice at different ages. At 3 weeks, ovaries contain various stages of follicles, including primary, secondary, and antral follicles in wild-type animals (Fig. 2*a*) (19). In $AR^{-/-}$ ovaries at 3 weeks of age, the folliculogenesis appeared to be unaltered, with normal numbers and localization of primary and secondary follicles (Fig. 2 *a* and *e*). However, degenerated folliculogenesis became evident with further aging. Although follicles and corpora lutea at all developmental stages were still present, corpora lutea numbers were clearly reduced in 8-week-old $AR^{-/-}$ mutants (Fig. 2 *b* and *f*), similar to that observed in another mouse line (20). Expected apoptosis was seen in atretic follicles by activated caspase-3 immunohistochemistry assays (Fig. 2*i*). But, by 32 weeks of age, defects in folliculogenesis in $AR^{-/-}$ ovaries became profound, with fewer follicles observed and increased atretic follicles (Fig. 2 *c* and *g*), and >40% (5 of 12 mice) of the $AR^{-/-}$ females were already infertile. By 40 weeks, all $AR^{-/-}$ females became infertile, with no follicles remaining (Fig. 2 *d* and *h*); at the same age, $AR^{+/+}$ females were fertile and had normal follicle numbers. Consistent with progressive deficiency in folliculogenesis, the pup number per litter steadily decreased in aging $AR^{-/-}$ females (Fig. 2*i*). These data indicate that AR plays an important physiological role at the preluteal phase of folliculogenesis.

Alteration in Gene Expressions of Several Major Regulators Involved in the Oocyte–Granulosa Cell Regulatory Loop. To explore the molecular basis underlying the impaired folliculogenesis in $AR^{-/-}$ ovaries, we analyzed expression of several major known regulators and markers of folliculogenesis (21–23). Surprisingly, no significant alterations in mRNA levels of LH receptor (*Lhr*), FSH receptor (*Fshr*), p450 side chain cleavage enzyme (*Cyp11a1*), 17-α-hydroxylase (*Cyp17a1*), aromatase (*Cyp19*), estrogen receptor-β (*Esr2*), cyclin D2 (*Ccnd2*), or insulin-like growth factor 1 (*Igf1*) of 8-week-old $AR^{-/-}$ ovaries at the proestrus stage, and further cyclooxygenase 2 (*Ptgs2*) or progesterone receptor (*Pgr*) at the estrus stage, were detected by

PHYSIOLOGY

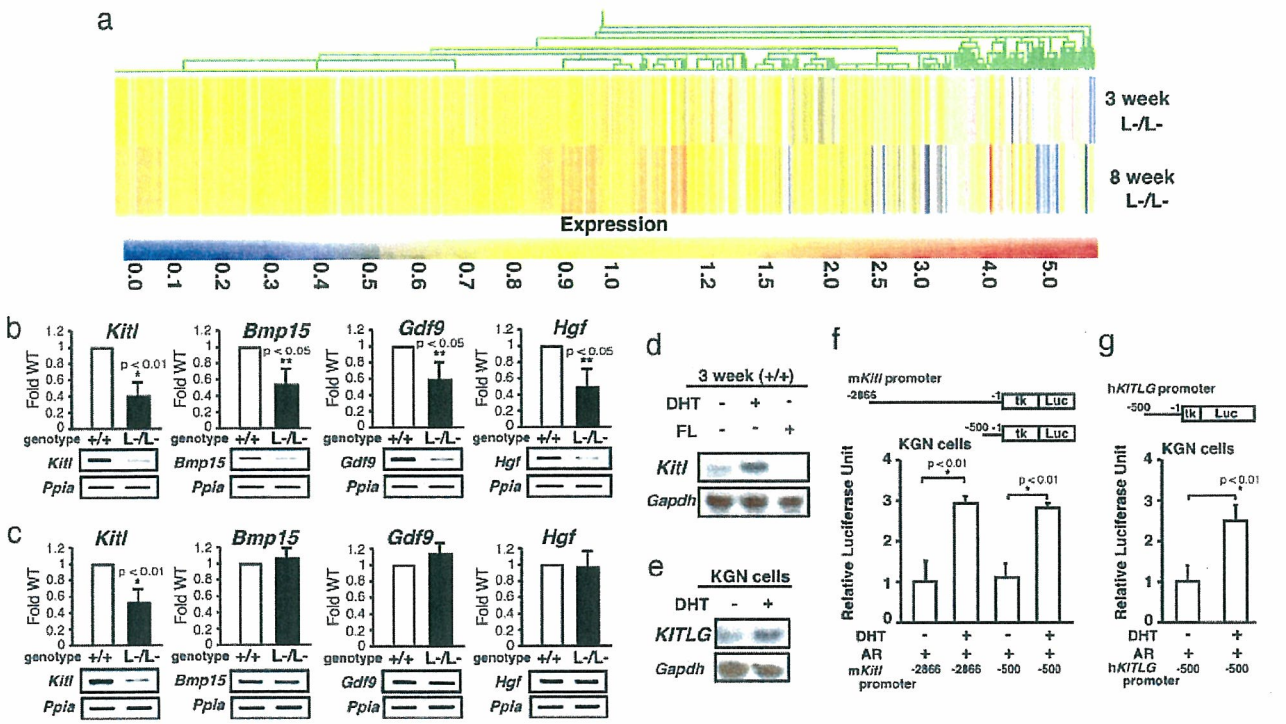

Fig. 4. Genome-wide microarray analysis and semiquantitative RT-PCR revealed that expression of the oocyte–granulosa cell regulator loop was down-regulated in $AR^{-/-}$ ovaries. (*a*) Microarray analysis of $AR^{-/-}$ compared with $AR^{+/+}$ ovaries at 3 and 8 weeks of age. Data obtained from microarray analysis as described in *Materials and Methods* were used to generate a cluster analysis. Each vertical line represents a single gene. The ratios of gene expression levels in $AR^{-/-}$ ovaries compared with wild type are presented. (*b* and *c*) Semiquantitative RT-PCR analysis of AR-regulated genes identified from the microarray study. Results shown are representative (using one ovary per genotype in each experiment) of five independent experiments. Data are shown as mean ± SEM and were analyzed by using Student's *t* test. (*d*) Comparison of *Kitl* gene expression by Northern blot analysis among placebo-, DHT-, and flutamide (FL)-treated $AR^{+/+}$ mouse ovaries. (*e*) Induction of *KITLG* gene expression by DHT treatment in KGN cells. (*f* and *g*) Androgen responsiveness in the mouse and human *kit ligand* promoters by a luciferase assay performed by using KGN cells. Data are shown as mean ± SEM and were analyzed by using Student's *t* test.

semiquantitative RT-PCR analysis (Fig. 3). Genome-wide microarray analysis (17) of RNA from 8-week-old $AR^{-/-}$ ovaries at the proestrus stage has been undertaken to identify AR-regulated genes. In comparison with $AR^{+/+}$ ovaries, expressions of 772 genes were down-regulated, whereas 351 genes were up-regulated in $AR^{-/-}$ ovaries (Fig. 4*a*; see also Tables 1 and 2, which are published as supporting information on the PNAS web site). Several genes known to be involved in the oocyte–granulosa cell regulatory loop (24) were identified as candidate AR target genes, including KIT ligand (*Kitl*) (25), morphogenetic protein 15 (*Bmp15*) (26), growth differentiation factor-9 (*Gdf9*) (27), and hepatocyte growth factor (*Hgf*) (28). Impaired folliculogenesis had been reported in mice deficient in each of these three regulators (26, 27, 29). To validate the microarray data, we performed semiquantitative RT-PCR analysis of 8-week-old $AR^{-/-}$ ovary RNA and confirmed that expression of these factors was down-regulated (Fig. 4*b*). To identify a regulator downstream of the AR signaling at an earlier stage of folliculogenesis, 3-week-old $AR^{-/-}$ ovaries that, as pointed out earlier, display no apparent phenotypic abnormality were examined. Fewer genes had altered expression levels (519 genes up-regulated; 326 genes down-regulated) (Fig. 4*a*; see also Tables 3 and 4, which are published as supporting information on the PNAS web site), and, of the four regulators tested by RT-PCR, only *Kitl* was found to be down-regulated at this age (Fig. 4*c*). Because *Kitl* is a granulosa cell-derived factor and stimulates oocyte growth and maturation (29–31), down-regulation of the *Kitl* expression in 3-week-old or even younger $AR^{-/-}$ ovaries may trigger impairment in folliculogenesis at a later age. To test for possible *Kitl* gene regulation by AR, 3-week-old wild-type females were treated with 5α-dihydrotestosterone (DHT). At 4 h after hormone injection, a clear induction of *Kitl* expression was observed in the ovaries, whereas a known antiandrogen flutamide attenuated the induction by DHT (Fig. 4*d*). The induction of endogenous human *kit ligand* (*KITLG*) gene by DHT was also observed in human granulosa-like tumor cells (KGN) in culture (Fig. 4*e*). Furthermore, androgen-induced transactivation of mouse and human *kit ligand* promoters (32) was observed by a luciferase reporter assay (33) in KGN (Fig. 4 *f* and *g*), 293T, and HeLa (data not shown) cells. However, no response to DHT was detected in the similar assay using promoters of the *Bmp15*, *Gdf9*, and *Hgf* genes (data not shown). Thus, we have shown that, in a regulatory cascade controlling folliculogenesis, *Kitl* represents a direct downstream target of androgen signaling.

As an upstream regulator, AR may also be indirectly involved in control of expression of other genes critical for folliculogenesis, because an age-dependent down-regulation of *Bmp15*, *Gdf9*, and *Hgf* gene expression was also observed in $AR^{-/-}$ ovaries. *Bmp15* and *Gdf9* are oocyte-derived factors that promote the development of surrounding granulosa cells in growing follicles (34, 35), whereas *Hgf* is secreted by theca cells and acts as a granulosa cell growth factor (36). Down-regulation of these factors, presumably due to decreased *Kitl* expression, may lead to impaired bidirectional communication between oocyte and granulosa cells (24) and, eventually, to early termination of folliculogenesis, as in POF syndrome.

Thus, we have identified AR as a novel regulator of follicu-

logenesis that apparently acts in the regulatory cascade upstream of the major factors controlling ovarian function, confirming the previous findings of the AR expression in granulose cells of growing follicles (3). Although not immediately relevant to the ovarian physiology, abnormal development of the mammary glands observed in our AR-deficient mice adds further strong evidence of an essential role of the AR not only in male, but also in female, reproductive function.

With increasing age of the first childbirth by women in the modern society, POF syndrome has become an important social and medical problem. Our findings suggest that POF syndrome may be caused by an impairment in androgen signaling and that X chromosomal mutations affecting the *AR* gene function may play a key role in hereditary POF. From clinical perspective, the present study provides evidence that AR can be a beneficial therapeutic target in treatment of POF syndrome patients.

We thank T. Iwamori and H. Tojo for expert advice on mammary gland anatomy, Y. Kanai for ovarian phenotypic analysis, members of the KO project team at the laboratory of Nuclear Signaling (Institute of Molecular and Cellular Biosciences) for their support, A. P. Kouzmenko for helpful suggestions, and H. Higuchi for manuscript preparation. This work was supported in part by the Program for Promotion of Basic Research Activities for Innovative Biosciences and priority areas from the Ministry of Education, Culture, Sports, Science, and Technology (to S.K.).

1. Laml, T., Preyer, O., Umek, W., Hengstschlager, M. & Hanzal, H. (2002) *Hum. Reprod. Update* **8,** 483–491.
2. Davison, R. M., Davis, C. J. & Conway, G. S. (1999) *Clin. Endocrinol. (Oxford)* **51,** 673–679.
3. Tetsuka, M., Whitelaw, P. F., Bremner, W. J., Millar, M. R., Smyth, C. D. & Hillier, S. G. (1995) *J. Endocrinol.* **145,** 535–543.
4. Ehrmann, D. A., Barnes, R. B. & Rosenfield, R. L. (1995) *Endocr. Rev.* **16,** 322–353.
5. Norman, R. J. (2002) *Mol. Cell. Endocrinol.* **191,** 113–119.
6. Kato, S. (2002) *Clin. Pediatr. Endocrinol.* **11,** 1–7.
7. Sato, T., Matsumoto, T., Kawano, H., Watanabe, T., Uematsu, Y., Sekine, K., Fukuda, T., Aihara, K., Krust, A., Yamada, T., *et al.* (2004) *Proc. Natl. Acad. Sci. USA* **101,** 1673–1678.
8. Sato, T., Matsumoto, T., Yamada, T., Watanabe, T., Kawano, H. & Kato, S. (2003) *Biochem. Biophys. Res. Commun.* **300,** 167–171.
9. Kawano, H., Sato, T., Yamada, T., Matsumoto, T., Sekine, K., Watanabe, T., Nakamura, T., Fukuda, T., Yoshimura, K., Yoshizawa, T., *et al.* (2003) *Proc. Natl. Acad. Sci. USA* **100,** 9416–9421.
10. Li, M., Indra, A. K., Warot, X., Brocard, J., Messaddeq, N., Kato, S., Metzger, D. & Chambon, P. (2000) *Nature* **407,** 633–636.
11. Sekine, K., Ohuchi, H., Fujiwara, M., Yamasaki, M., Yoshizawa, T., Sato, T., Yagishita, N., Matsui, D., Koga, Y., Itoh, N. & Kato, S. (1999) *Nat. Genet.* **21,** 138–141.
12. Yoshizawa, T., Handa, Y., Uematsu, Y., Takeda, S., Sekine, K., Yoshihara, Y., Kawakami, T., Arioka, K., Sato, H., Uchiyama, Y., *et al.* (1997) *Nat. Genet.* **16,** 391–396.
13. Gubbay, J., Collignon, J., Koopman, P., Capel, B., Economou, A., Munsterberg, A., Vivian, N., Goodfellow, P. & Lovell-Badge, R. (1990) *Nature* **346,** 245–250.
14. Yanagisawa, J., Yanagi, Y., Masuhiro, Y., Suzawa, M., Watanabe, M., Kashiwagi, K., Toriyabe, T., Kawabata, M., Miyazono, K. & Kato, S. (1999) *Science* **283,** 1317–1321.
15. Britt, K. L., Drummond, A. E., Cox, V. A., Dyson, M., Wreford, N. G., Jones, M. E., Simpson, E. R. & Findlay, J. K. (2000) *Endocrinology* **141,** 2614–2623.
16. Ohtake, F., Takeyama, K., Matsumoto, T., Kitagawa, H., Yamamoto, Y., Nohara, K., Tohyama, C., Krust, A., Mimura, J., Chambon, P., *et al.* (2003) *Nature* **423,** 545–550.
17. Fujimoto, N., Igarashi, K., Kanno, J., Honda, H. & Inoue, T. (2004) *J. Steroid Biochem. Mol. Biol.* **91,** 121–129.
18. Couse, J. F. & Korach, K. S. (1999) *Endocr. Rev.* **20,** 358–417.
19. Elvin, J. A. & Matzuk, M. M. (1998) *Rev. Reprod.* **3,** 183–195.
20. Hu, Y. C., Wang, P. H., Yeh, S., Wang, R. S., Xie, C., Xu, Q., Zhou, X., Chao, H. T., Tsai, M. Y. & Chang, C. (2004) *Proc. Natl. Acad. Sci. USA* **101,** 11209–11214.
21. Elvin, J. A., Yan, C., Wang, P., Nishimori, K. & Matzuk, M. M. (1999) *Mol. Endocrinol.* **13,** 1018–1034.
22. Zhou, J., Kumar, T. R., Matzuk, M. M. & Bondy, C. (1997) *Mol. Endocrinol.* **11,** 1924–1933.
23. Burns, K. H., Yan, C., Kumar, T. R. & Matzuk, M. M. (2001) *Endocrinology* **142,** 2742–2751.
24. Matzuk, M. M., Burns, K. H., Viveiros, M. M. & Eppig, J. J. (2002) *Science* **296,** 2178–2180.
25. Joyce, I. M., Pendola, F. L., Wigglesworth, K. & Eppig, J. J. (1999) *Dev. Biol.* **214,** 342–353.
26. Yan, C., Wang, P., DeMayo, J., DeMayo, F. J., Elvin, J. A., Carino, C., Prasad, S. V., Skinner, S. S., Dunbar, B. S., Dube, J. L., *et al.* (2001) *Mol. Endocrinol.* **15,** 854–866.
27. Dong, J., Albertini, D. F., Nishimori, K., Kumar, T. R., Lu, N. & Matzuk, M. M. (1996) *Nature* **383,** 531–535.
28. Parrott, J. A., Vigne, J. L., Chu, B. Z. & Skinner, M. K. (1994) *Endocrinology* **135,** 569–575.
29. Driancourt, M. A., Reynaud, K., Cortvrindt, R. & Smitz, J. (2000) *Rev. Reprod.* **5,** 143–152.
30. Huang, E. J., Manova, K., Packer, A. I., Sanchez, S., Bachvarova, R. F. & Besmer, P. (1993) *Dev. Biol.* **157,** 100–109.
31. Packer, A. I., Hsu, Y. C., Besmer, P. & Bachvarova, R. F. (1994) *Dev. Biol.* **161,** 194–205.
32. Grimaldi, P., Capolunghi, F., Geremia, R. & Rossi, P. (2003) *Biol. Reprod.* **69,** 1979–1988.
33. Kitagawa, H., Fujiki, R., Yoshimura, K., Mezaki, Y., Uematsu, Y., Matsui, D., Ogawa, S., Unno, K., Okubo, M., Tokita, A., *et al.* (2003) *Cell* **113,** 905–917.
34. Otsuka, F. & Shimasaki, S. (2002) *Proc. Natl. Acad. Sci. USA* **99,** 8060–8065.
35. Joyce, I. M., Clark, A. T., Pendola, F. L. & Eppig, J. J. (2000) *Biol. Reprod.* **63,** 1669–1675.
36. Parrott, J. A. & Skinner, M. K. (1998) *Endocrinology* **139,** 2240–2245.

Antitumor Activity of ZSTK474, a New Phosphatidylinositol 3-Kinase Inhibitor

Shin-ichi Yaguchi, Yasuhisa Fukui, Ichiro Koshimizu, Hisashi Yoshimi, Toshiyuki Matsuno, Hiroaki Gouda, Shuichi Hirono, Kanami Yamazaki, Takao Yamori

Background: **We previously synthesized a novel *s*-triazine derivative, ZSTK474 [2-(2-difluoromethylbenzimidazol-1-yl)-4,6-dimorpholino-1,3,5-triazine], that strongly inhibited the growth of tumor cells. We identified its molecular target, investigated its effects on cellular signaling pathways, and examined its antitumor efficacy and toxicity in vivo.** ***Methods:*** **We used COMPARE analysis of chemosensitivity measurements from 39 human cancer cell lines and identified phosphatidylinositol 3-kinase (PI3K) as a molecular target for ZSTK474. PI3K was immunoprecipitated from A549 cell lysates, and its activity was measured by assessing the incorporation of ^{32}P into phosphatidylinositol. We used the crystal structure of the PI3K–LY294002 complex to model the binding of ZSTK474 to PI3K (where LY294002 is a known PI3K inhibitor). PI3K downstream activity was analyzed by immunoblotting. Antitumor activity of ZSTK474 was examined against A549, PC-3, and WiDr xenografts in nude mice. Phosphorylation of Akt, a serine/threonine protein kinase and a major signaling component downstream of PI3K, was assessed in vivo by immunohistochemistry.** ***Results:*** **PI3K was identified as a molecular target for ZSTK474 by COMPARE analysis. We confirmed that ZSTK474 directly inhibited PI3K activity more efficiently than the PI3K inhibitor LY294002. At concentrations of 1 μM, ZSTK474 and LY2194002 reduced PI3K activity to 4.7% (95% confidence interval [CI] = 3.2% to 6.1%) and 44.6% (95% CI = 38.9% to 50.3%), respectively, of the untreated control level. Molecular modeling of the PI3K–ZSTK474 complex indicated that ZSTK474 could bind to the ATP-binding pocket of PI3K. ZSTK474 inhibited phosphorylation of signaling components downstream from PI3K, such as Akt and glycogen synthase kinase 3β, and mediated a decrease in cyclin D1 levels. ZSTK474 administered orally to mice had strong antitumor activity against human cancer xenografts without toxic effects in critical organs. Akt phosphorylation was reduced in xenograft tumors after oral administration of ZSTK474.** ***Conclusion:*** **ZSTK474 is a new PI3K inhibitor with strong antitumor activity against human cancer xenografts without toxic effects in critical organs. ZSTK474 merits further investigation as an anticancer drug. [J Natl Cancer Inst 2006;98:545–56]**

Phosphatidylinositol 3-kinase (PI3K), which is active in signal transduction, generates phosphatidylinositol-3,4,5-trisphosphate (PIP_3) by phosphorylating phosphatidylinositol-4,5-bisphosphate *(1,2)*. PI3K is involved in various cellular processes, including cell survival, vesicle transport, and cytoskeletal rearrangement *(3,4)*. The importance of PI3K in tumorigenesis is supported by the following evidence. The chicken retrovirus ASV16 carries an oncogenic PI3K gene *(5)*, and mutation and/or amplification of PI3K genes *(6–10)* has been reported in human and other mammalian cancer cells. Constitutive activation of PI3K may contribute to the malignant phenotype of signet ring carcinomas *(11)*, and PTEN, a PIP_3 phosphatase, has been identified as a tumor suppressor gene *(12)*.

Many clinical studies also indicate that deregulation of PI3K pathway plays a role in various cancers *(3,7)* and that PI3K may thus be a good target for anticancer drug development *(3)*. Validation of PI3K as a good target for drug development began with the use of dominant-negative mutants and RNA interference studies *(13,14)*. Indeed, a number of compounds have been identified that inhibit PI3K, including wortmannin *(15,16)*, which was originally isolated from soil bacteria and is toxic to fungi; the closely related viridin analogues *(17,18)*; and LY294002, a morpholino derivative of the broad-spectrum kinase inhibitor quercetin *(19)*. Because of inherent difficulties with the stability, solubility, and toxicity of these compounds, efforts are under way to develop new inhibitors of the PI3K pathway *(20,21)*.

In previous work, we synthesized a chemical library of *s*-triazine derivatives and screened these compounds for their ability to inhibit tumor cell growth *(22,23)*. Among more than 1500 *s*-triazine derivatives, we found a new compound, ZSTK474 [2-(2-difluoromethylbenzimidazol-1-yl)-4,6-dimorpholino-1,3,5-triazine], that showed strong antiproliferative activity. However, its molecular target or its potential for a novel anticancer drug was unknown.

We previously established a panel of 39 human cancer cell lines (termed JFCR39) coupled to a drug activity database *(24–26)* that is comparable to the panel developed by the National

Affiliations of authors: Division of Molecular Pharmacology, Cancer Chemotherapy Center, Japanese Foundation for Cancer Research, Ariake, Koto-ku, Tokyo, Japan (SY, KY, TY); Research Laboratory, Zenyaku Kogyo Co., Ltd., Ohizumi-machi, Nerima-ku, Tokyo, Japan (SY, IK, HY, TM); Laboratory of Biological Chemistry, Department of Applied Biological Chemistry, Faculty of Agricultural and Life Science, Graduate School of Agricultural and Life Science, University of Tokyo, Yayoi, Bunkyo-ku, Tokyo, Japan (YF); The School of Pharmaceutical Sciences, Kitasato University, Shirokane, Minato-ku, Tokyo, Japan (HG, SH).

Correspondence to: Takao Yamori, PhD, Division of Molecular Pharmacology, Cancer Chemotherapy Center, Japanese Foundation for Cancer Research, 3-10-6 Ariake, Koto-ku, Tokyo 135-8550, Japan (e-mail: yamori@jfcr.or.jp).

See "Notes" following "References."

DOI: 10.1093/jnci/djj133

Cancer Institute *(27,28)*. We compared cell growth inhibition profiles against the JFCR39 (herein termed fingerprints) of more than 60 standard drugs including doxorubicin, fluorouracil, cytarabine, methotrexate, vincristine, cisplatin, paclitaxel, and irinotecan, by using COMPARE analysis *(26)*, and we showed that COMPARE analysis is an information-intensive approach to identifying the molecular target of a new compound, as described by Paull et al. *(28)*. This system can be used to predict the molecular target or the mode of action of test compounds by assessing the correlation coefficient between the fingerprints mediated by such test compounds and by various reference compounds with known modes of action, including PI3K inhibitors.

The purpose of this study was to identify the molecular target of ZSTK474 with the aid of COMPARE analysis, to investigate the effects of ZSTK474 on cellular signaling pathways, and to examine the antitumor efficacy and toxicity of ZSTK474 in vivo.

Materials and Methods

Chemicals

ZSTK116, ZSTK474, ZSTK781, and ZSTK1178 were synthesized in the Research Laboratory, Zenyaku Kogyo Co., Ltd. (Tokyo, Japan). For in vitro studies, these compounds were dissolved in dimethyl sulfoxide. ZSTK474 was suspended in 5% hydroxypropylcellulose in water as a solid dispersion form for animal experiments. Other anticancer drugs and chemicals were purchased as follows: doxorubicin and 5-fluorouracil from Kyowa Hakko Kogyo (Tokyo, Japan); cisplatin from Nippon Kayaku (Tokyo, Japan); irinotecan from Yakult Honsha (Tokyo, Japan); and wortmannin, LY294002, tetramethylrhodamine isothiocyanate-conjugated phalloidin, Igepal CA-630, and platelet-derived growth factor from Sigma (St. Louis, MO).

Cell Lines

A panel of 39 human cancer cell lines (termed JFCR39) *(25,26)* and B16F10 melanoma cells *(29)* were previously described. All cell lines were cultured in RPMI 1640 medium supplemented with 5% fetal bovine serum, penicillin (100 U/mL), and streptomycin (100 μg/mL) at 37 °C in humidified air containing 5% CO_2. Cell lines OVCAR3, A549, PC-3, and WiDr, which were used for in vitro detailed analysis or for in vivo study, originated from an ovarian cancer, non–small-cell lung cancer, prostate cancer, and colon cancer, respectively. For in vivo study, A549, PC-3, and WiDr were grown as subcutaneous tumors in nude mice.

Analysis of Cell Proliferation Inhibition

The inhibition of cell proliferation was assessed by measuring changes in total cellular protein in a culture of each cell line in the JFCR panel of cell lines after 48 hours of drug treatment by use of a sulforhodamine B assay *(30)*. The 50% growth inhibition (GI_{50}) value of the drug was calculated as described previously *(26,27)*. The graphic representation of a drug's mean differential growth inhibition for the cell line panel was based on a calculation that used a set of GI_{50} values, as described previously *(28,31)*. To analyze the correlation between the mean graphs of drug A and drug B, the COMPARE computer algorithm was developed as previously described by Paull et al. *(28)*. The Pearson correlation coefficient between the mean graphs of drug A and drug B was calculated (n = 39).

PI3K Assay in Tumor Cell Extracts

The PI3K assay has been previously described by Fukui et al. *(32)*. In brief, A549 cells were lysed in a buffer containing 20 mM Tris–HCl (pH 7.5), 150 mM NaCl, 5 mM EDTA, and 1% Igepal CA-630 (Sigma), the lysates were centrifuged at 20 000*g* and 4 °C for 10 minutes, and the supernatants were used as cell lysate (protein = 2–4 mg/mL). To immunoprecipitate PI3K, we incubated 200 μL of cell lysate with anti-p85 polyclonal antibody (1 : 200 dilution; Upstate, Charlottesville, VA) and protein G–agarose (5 μL; Upstate). The anti-p85 polyclonal antibody recognizes the p85 regulatory subunit of PI3K. Class Ia catalytic subunits of PI3K (p110α, p110β, and p110δ) constitutively associate with the p85 subunit. Therefore, PI3Kα, PI3Kβ, and PI3Kδ can be immunoprecipitated by the anti-p85 polyclonal antibody. Agarose beads containing immunoprecipitates were washed twice with buffer A (20 mM Tris–HCl at pH 7.5, 150 mM NaCl, 5 mM EDTA, and 1% Igepal CA-630), once with buffer B (500 mM LiCl and 100 mM Tris–HCl at pH 7.5), once with distilled water, and once with buffer C (100 mM NaCl and 20 mM Tris–HCl at pH 7.5). Immunoprecipitates were suspended in 20 μL of buffer C containing phosphatidylinositol at 200 μg/mL. The mixture was preincubated with or without ZSTK474, LY294002, or wortmannin, as indicated, at 25 °C for 5 minutes. [γ-^{32}P]ATP (2 μCi per assay mixture; final concentration, 20 μM) and $MgCl_2$ (final concentration, 20 mM) were added to start the reaction. The reaction mixture was incubated at 25 °C for 20 minutes. During this incubation, formation of phosphatidylinositol-3-phosphate was linear (data not shown). Phosphorylated products of phosphatidylinositol were separated by thin-layer chromatography and visualized by autoradiography. The phosphatidylinositol-3-phosphate region was scraped from the plate, and radioactivity was also measured with liquid scintillation spectroscopy (LS6500 Scintillation System; Beckman Instruments, Fullerton, CA). The level of inhibition for each compound was determined as the percentage of ^{32}P counts per minute obtained without the test compound. To asses the reversibility of PI3K inhibition, the PI3K immunoprecipitates were treated with 1 μM ZSTK474, 10 μM LY294002, or 0.1 μM wortmannin for 5 minutes, and the reaction mixture was divided into two aliquots. One aliquot was washed four times with a buffer containing 100 mM NaCl and 20 mM Tris–HCl (pH 7.5) to remove free ZSTK474, LY294002, or wortmannin from the PI3K, and the PI3K activity of the washed precipitate was measured. The PI3K activity of the other aliquot was measured without washing.

PI3K Assay for Recombinant Catalytic Subunits of PI3K

PI3K assay for recombinant p110, the catalytic subunit of PI3K, was described previously by Gray et al. *(33)*. In a reaction volume of 20 μL, human p110 isoforms β, -γ, or -δ (Upstate) were incubated with 10 μM phosphatidylinositol-4,5-bisphosphate and 10 μM ATP in assay buffer for 30 minutes at room temperature. Stop buffer (5 μL) containing EDTA and biotinylated PIP_3 was added, followed by 5 μL of detection buffer containing europium-labeled anti–glutathione *S*-transferase (GST) monoclonal antibody, GST-tagged general receptor for phosphoinositides (GRP1) PH domain, and streptavidin allophycocyanin. Plus

and minus kinase control wells were also included. The plate was read in the time-resolved fluorescence mode, and the homogenous time-resolved fluorescence (HTRF) signal was determined according to the following formula: HTRF = 10 000 × (emission at 665 nm/emission at 620 nm).

Molecular Modeling of the PI3K–ZSTK474 Complex

Conformational analysis of ZSTK474 was performed first with the FlexX docking program *(34)*, which was used to construct a model of the PI3K–ZSTK474 complex structure. This program treats ring systems, such as the morpholino groups in ZSTK474, as rigid structures. The conformational analysis was done with the CAMDAS, version 2.1, program (conformational analyzer with molecular dynamics and sampling) *(35)*. Conditions used for CAMDAS calculation were similar to those described previously *(36)*. Twelve dihedral angles with respect to two morpholino rings were used to cluster similar conformations. As a result of the CAMDAS calculation, 64 different conformers were obtained.

The crystal structure of the PI3K–LY294002 complex (Protein Data Bank Identification Code 1E7V) was used to obtain the PI3K template structure for docking. The docking calculation of each ZSTK474 conformation with PI3K was performed with the FlexX program. A total of 10 482 different docking models were generated. Each docking model was then evaluated with the following five different score functions: the F-score *(34)*, the D-score *(37)*, the G-score *(38)*, the ChemScore *(39)*, and the PMF-score *(40)*. These functions were implemented in the SYBYL C-Score module. Finally, a new index, termed the average of auto-scaled score, was calculated to rank all docking models. This index has been recently defined in our laboratory to more adequately rank docking models *(41)*. In the top 20 docking models that were ranked according to the average of auto-scaled scores, all ZSTK474 molecules were found to similarly interact with PI3K. The only difference among the 20 models was with respect to the conformation of the two morpholino rings of ZSTK474. Therefore, we present one of these 20 models, in which two morpholino rings of ZSTK474 take a chair conformation, because this model has the lowest internal energy.

Assay for Chromatin Condensation

OVCAR3 cells were cultured in RPMI 1640 medium supplemented with 5% fetal bovine serum for 24 hours and then cultured for 48 hours with or without 10 μM ZSTK474. Cells were collected, fixed in 1% glutaraldehyde in phosphate-buffered saline (PBS) at 4 °C for 24 hours, stained with 167 μM Hoechst 33342 (Sigma), and examined by fluorescence microscopy to identify apoptotic cells.

Flow Cytometry Analysis

Cells were harvested, washed with ice-cold PBS, and fixed in 70% ethanol. Cells were then washed twice with ice-cold PBS again, treated with RNase A (500 μg/mL; Sigma) at 37 °C for 1 hour, and stained with propidium iodide (25 μg/mL; Sigma). The DNA content of the cells was analyzed with a flow cytometer (FACScalibur, Becton Dickinson, Franklin Lakes, NJ).

Membrane Ruffling

Murine embryonic fibroblasts were treated with or without 1 μM ZSTK474 for 15 minutes and then stimulated with platelet-derived growth factor (10 ng/mL) for 5 minutes. Cells were fixed with 3% formaldehyde at room temperature for 30 minutes and permeabilized with 0.1% Triton X-100 in PBS for 5 minutes. Filamentous actin in cells was stained with tetramethylrhodamine isothiocyanate-conjugated phalloidin at 0.1 μg/mL, and cells were examined by fluorescence microscopy.

Analysis of PIP_3 Production

PIP_3 production in intact cells was measured as described previously by Kimura et al. *(42)*. In brief, to label murine embryonic fibroblasts, medium was replaced with prewarmed phosphate-free Dulbecco's modified Eagle medium with 25 mM HEPES (pH 7.4) containing [^{32}P]orthophosphate (0.1 mCi/mL), and cultures were incubated at 37 °C for 4 hours. Lipids were extracted with chloroform and separated by thin-layer chromatography. PIP_3 spots were visualized by autoradiography and identified by standards synthesized by PI3K in vitro (data not shown). Radioactivity in the spots was quantitated with a PhosphorImager SI system (Molecular Dynamics, Sunnyvale, CA).

Western Blot Analysis

A549 cells were lysed in a buffer containing 10 mM Tris–HCl at pH 7.4, 50 mM NaCl, 50 mM NaF, 30 mM sodium pyrophosphate, 50 mM Na_3VO_4, 5 mM EDTA, aprotinin at 100 Kal U/mL, 1 mM phenylmethylsulfonyl fluoride, 0.5% Nonidet P-40, and 0.1% sodium dodecyl sulfate. Proteins in cell lysates were separated by sodium dodecyl sulfate–polyacrylamide gel electrophoresis followed by electroblotting onto a polyvinylidene difluoride membrane (Amersham Biosciences, Piscataway, NJ). Rabbit polyclonal antibodies for Akt, phosphorylated Akt (phosphorylated residue Ser-473), phosphorylated glycogen synthase kinase 3β (GSK-3β; phosphorylated residue Ser-9), phosphorylated FKHR (phosphorylated residue Thr-24)/phosphorylated FKHRL1 (phosphorylated residue Thr-32), phosphorylated TSC-2 (phosphorylated residue Ser-1462), phosphorylated mTOR (phosphorylated residue Ser-2448), phosphorylated p70S6K (phosphorylated residue Thr-389), phosphorylated MEK1/2 (phosphorylated residues Ser-217/221), and phosphorylated ERK1/2 (phosphorylated residues Thr-202/Tyr-204) were purchased from Cell Signaling Technology (Beverly, MA) and were diluted 1 : 1000. Rabbit anti–cyclin D1 polyclonal antibody (1 : 200 dilution) was purchased from BioSource International (Camarillo, CA). Horseradish peroxidase–conjugated goat anti–rabbit immunoglobulin G (Cell Signaling Technology) was used as a secondary antibody. Immunoreactive bands were identified with the ECL-plus Western Blotting Detection System (Amersham Biosciences).

Animal Experiments

Animal care and treatment was performed in accordance with the guidelines of the animal use and care committee of the Research Laboratory, Zenyaku Kogyo, and conformed to the NIH *Guide for the Care and Use of Laboratory Animals*. All procedures were approved by the above committee. Male BDF_1 mice and female nude mice with BALB/c genetic backgrounds were purchased from Charles River Japan, Inc. (Yokohama, Japan). Mice were maintained under specific pathogen–free conditions and provided with sterile food and water ad libitum. We used 56 BDF_1 mice. Each BDF_1 mouse was subcutaneously

injected with 5×10^5 B16F10 melanoma cells. Seven days after inoculation, animals were divided randomly into test groups (each with seven mice), and the administration of the drugs, as indicated, began (day 0). ZSTK474 at 100, 200, or 400 mg/kg of body weight was orally administered daily from days 0 to 13. Reference drugs were irinotecan, cisplatin, doxorubicin, and 5-fluorouracil. Each reference drug was administered intravenously from day 0 at the maximum tolerable dose by use of the following optimal schedules: irinotecan at 100 mg/kg administered on days 0, 3, and 7; cisplatin at 10 mg/kg on day 0; doxorubicin at 12 mg/kg on day 0; and 5-fluorouracil at 50 mg/kg on days 0, 3, and 7. Human tumor xenografts were generated with A549 lung cancer cells, PC-3 prostate cancer cells, and WiDr colon cancer cells and were grown as subcutaneous tumors in nude mice. Forty-five nude mice were used in these experiments. Each nude mouse was subcutaneously inoculated with a tumor fragment of 3 mm × 3 mm × 3 mm. When tumors reached a volume of 100–300 mm^3, animals were divided randomly into test groups (each with five mice) (day 0). ZSTK474 (400 mg/kg) was administered orally from day 0 until day 13 except for days 3 and 10. For longer administration periods, ZSTK474 at 400 mg/kg was orally administered daily from days 0 to 26, except for days 6, 13, and 20. Then, the mice were photographed on day 28. In another experiment, ZSTK474 at a higher dosage of 800 mg/kg was orally administered in the same schedule, and the body weight changes of the mice were monitored to observe toxicity.

Measurement of Tumor Volume

The length (L) and width (W) of the subcutaneous tumor mass were measured by calipers in live mice, and the tumor volume (TV) was calculated as: $TV = (L \times W^2)/2$. The tumor volume at day n was expressed as relative tumor volume (RTV), according to the formula $RTV = TV_n/TV_0$, where TV_n is the tumor volume at day n, and TV_0 is the tumor volume at day 0. Tumor regression (T/C%) on day 14 was determined by use of the RTV values as follows: $T/C\% = 100 \times$ (mean RTV of treated group)/(mean RTV of control group). To assess toxicity, we measured the body weight of the tumor-bearing mice. After the chronic administration of ZSTK474, mice were subjected to necropsy examination, including the histopathologic evaluation of bone marrow.

Bone Marrow in Mice Femur

Right-side femurs were fixed with 10% neutral formalin and decalcified with Plank–Rychlo fluid *(43)*. After embedding in paraffin, 3-μm sections of bone marrow were stained with hematoxylin and eosin.

Immunohistochemistry

When the volume of tumors reached 100–300 mm^3, ZSTK474 at 400 mg/kg was orally administered once. Mice were killed 4 hours after ZSTK474 administration, and the tumors were excised. Tumor tissue was fixed in 10% neutral formalin and embedded in paraffin. The 6-μm sections were deparaffinized in xylene and then in a 100% to 50% ethanol series. Immunohistochemistry-specific phosphorylated Akt (phosphorylated on Ser-473) antibody and phosphorylated Akt (phosphorylated on Ser-473) blocking peptide were purchased from Cell Signaling Technology. The tissue sections were analyzed by immunohistochemistry for the expression of phosphorylated Akt (Ser-473). For control experiment, phosphorylated Akt (Ser-473) blocking peptide was incubated with phosphorylated Akt (Ser-473) antibody at 4 °C for 2 hours before incubating with the tissue section. The ABC method (Vectastain ABC system kit; Vector Laboratories, Burlingame, CA) was used for immunohistochemical staining, with the sections also being counterstained with hematoxylin.

Statistical Analysis

Pearson correlation coefficients were calculated for the COMPARE analysis and statistical correlation. The two-sided Mann–Whitney U test was used to test the statistical significance of the antitumor efficacy of ZSTK474 in relative tumor growth ratio on days 4, 7, 11, and 14. The number of samples is indicated in the description of each experiment. All statistical tests were two-sided.

Results

Measurement of the Growth-Inhibitory Activity of ZSTK474 and Identification of its Molecular Target

We synthesized and screened a chemical library of *s*-triazine derivatives based on their ability to mediate growth inhibition of tumor cells. We found that ZSTK474 showed potent antiproliferative activity. The chemical structure of ZSTK474 is shown in Fig. 1.

To identify potential molecular targets for ZSTK474, we used COMPARE analysis, an approach that is based on chemosensitivity measurements from the JFCR39 panel of cell lines. We treated cells in the JFCR39 panel with ZSTK474 and examined its effect on cell proliferation. In this way, we obtained the fingerprint for ZSTK474 (Fig. 2). The COMPARE analysis revealed that the fingerprint of ZSTK474 correlated with the fingerprints of noanticancer drug currently in use. However, the fingerprint of ZSTK474 did correlate statistically significantly with that of LY294002, a PI3K inhibitor ($r = .766$ and $P < .001$), as shown in Fig. 2, and with that of wortmannin, another well-characterized PI3K inhibitor ($r = .519$ and $P = .001$). Thus ZSTK474 appears to act as a PI3K inhibitor, although its structure is different from that of LY294002 or of wortmannin (Fig. 1).

We also compared the potency of ZSTK474 in cell growth inhibition with those of LY294002 and wortmannin. The mean logarithm of GI_{50} for ZSTK474 was −6.49 (at 0.32 μM ZSTK474), which was substantially lower than that observed with LY294002 (−5.13 at 7.4 μM) or wortmannin (−5.00 at 10 μM), indicating that ZSTK474 had stronger cell growth inhibitory activity than either of these two known PI3K inhibitors.

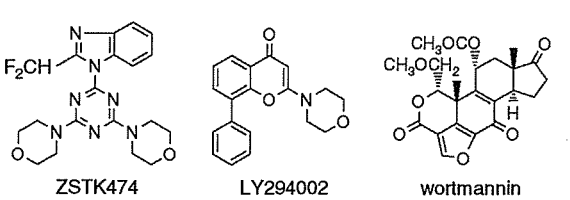

Fig. 1. Chemical structures of the phosphatidylinositol 3-kinase inhibitors ZSTK474, LY294002, and wortmannin. ZSTK474 has one 1-benzimidazolyl and two morpholino groups as substituents on the 1,3,5-triazine ring.

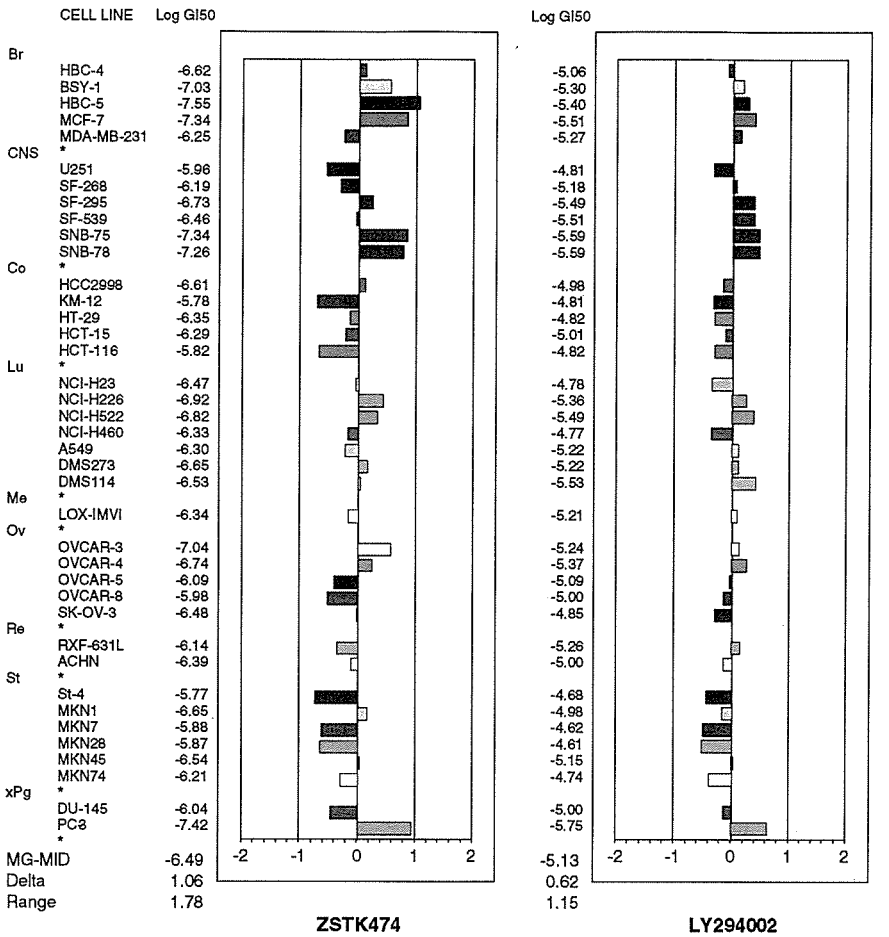

Fig. 2. Growth inhibition activity of ZSTK474 and LY294002 against a panel of 39 human cancer cell lines in the JFCR39 panel. Mean graph was produced by computer processing of the 50% growth inhibition (GI_{50}) values. Logarithm of the GI_{50} value for each cell line is indicated. In the plot, **columns to the right of zero** indicate that the sensitivity of the cell line to the compound, and **columns to the left** indicate resistance to the compound. The *x*-axis represents logarithm of difference between the mean of GI_{50} values for 39 cell lines and the GI_{50} value for each cell line in the JFCR39 panel. One scale represents one logarithm difference. MG-MID = mean of logarithm of GI_{50} values for 39 cell lines in the JFCR39 panel; Delta = logarithm of difference between the MG-MID and the logarithm of the GI_{50} value for the most sensitive cell line; Range = logarithm of difference between the logarithm of the GI_{50} value for the most resistant cell line and the logarithm of the GI_{50} value for the most sensitive cell line. Br = breast; CNS = central nervous system; Co = colon ; Lu = lung; Me = melanoma; Ov = ovarian; Re = renal; St = stomach; xPg = prostate. Each **hatch mark** corresponds to the cell line indicated to the left.

Inhibition of PI3K Activity by ZSTK474

We next examined the ability of ZSTK474 to inhibit PI3K activity. We selected A549 cells as the source of PI3K because these cells had an average level of sensitivity to ZSTK474 among cells in the JFCR39 panel. For these experiments, we used PI3K that had been immunoprecipitated from A549 cell lysates with an anti-p85 polyclonal antibody. ZSTK474 inhibited PI3K activity in a dose-dependent manner (Fig. 3, A). At concentrations of 1 μM, ZSTK474 and LY2194002 reduced the PI3K activity to 4.7% (95% confidence interval [CI] = 3.2% to 6.1%) and 44.6% (95% CI = 38.9% to 50.3%), respectively, of the untreated control activity. The respective concentrations of ZSTK474, LY294002, and wortmannin that inhibited 50% of the PI3K activity (IC_{50}) were 37, 790, and 11 nM. Therefore, as a PI3K inhibitor, ZSTK474 had a 20-fold greater activity than that of LY294002, but its activity was similar to that of wortmannin. However, ZSTK474 reversibly inhibited PI3K activity, as does LY294002, whereas wortmannin irreversibly inhibited PI3K activity (Fig. 3, B). ZSTK474 did not substantially inhibit the activity of 139 other protein kinases (Supplementary Table 1, available at http://jncicancerspectrum.oxfordjournals.org/jnci/content/vol98/issue8), indicating that ZSTK474 is highly specific to PI3K.

There are four subtypes of p110, the catalytic subunit of PI3K—α, β, γ, and δ. The specificity of ZSTK474 to these subtypes was of interest because a high frequency of mutations in the PIK3CA gene, encoding p110α, in human cancers has been recently reported *(7,8)*. With the PI3K assay described above, it was not possible to determine subtype specificity because the precipitates obtained with the anti-p85 polyclonal antibody could contain a mixture of p110α, -β, and -δ. To determine the subtype specificity of ZSTK474, we examined ZSTK474 for its activity against recombinant p110β, -γ, and -δ. We found that ZSTK474 inhibited the activities of p110β, -γ, and -δ, with respective IC_{50} values of 17, 53, and 6 nM (Supplementary Fig. 1 available at http://jncicancerspectrum.oxfordjournals.org/jnci/content/vol98/issue8), indicating that ZSTK474 was apparently not subtype specific.

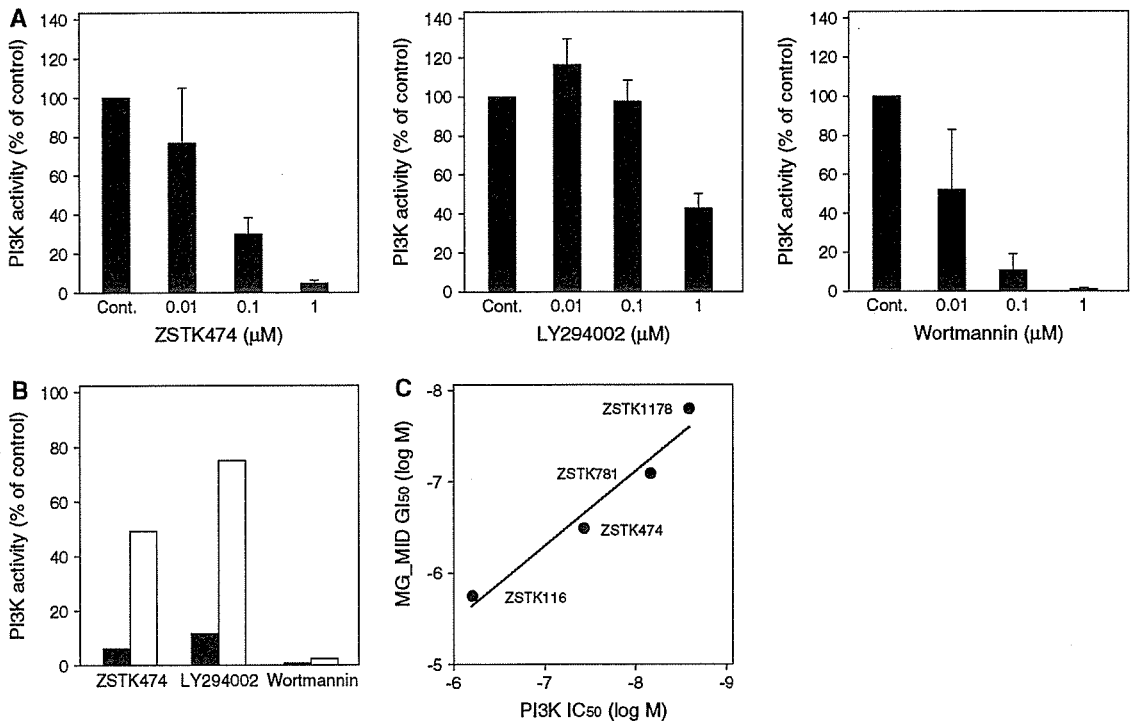

Fig. 3. Effect of ZSTK474 on phosphatidylinositol 3-kinase (PI3K) activity. A) Inhibition of PI3K activity. PI3K was immunoprecipitated from A549 cell lysates with anti-p85 polyclonal antibody, and immunoprecipitates were thoroughly washed sequentially with buffer A, buffer B, distilled water, and buffer C. After treatment of the PI3K immunoprecipitates with ZSTK474, LY294002, or wortmannin, as indicated, for 5 minutes, activity was measured by incubating PI3K immunoprecipitates with phosphatidylinositol and [γ-^{32}P]ATP. Phosphorylated derivatives of phosphatidylinositol were separated by thin-layer chromatography. The radioactivity in all derivatives was measured, and the results are expressed as the percentage of control untreated PI3K activity. Data are the mean of the results of two experiments performed in triplicate. Error bars = upper 95% confidence intervals. B) Reversibility of PI3K inhibition. The PI3K immunoprecipitates were treated with 1 μM ZSTK474, 10 μM LY294002, or 0.1 μM wortmannin for 5 minutes and divided into two aliquots. One aliquot was washed four times with a buffer containing 100 mM NaCl and 20 mM Tris–HCl (pH 7.5) to remove free ZSTK474, LY294002, or wortmannin from the PI3K, and PI3K activity of the washed precipitate was measured. The PI3K activity of the other aliquot was measured without washing. The PI3K activity of the immunoprecipitates with (**solid columns**) or without (**open columns**) washing is shown as the percentage of control untreated PI3K activity. Data are the mean of the results of two or three experiments. C) Activity of the *s*-triazine derivatives ZSTK116, ZSTK474, ZSTK781, and ZSTK1178. Scattered plot of concentrations of the various derivatives that inhibited 50% of PI3K activity (IC_{50}) versus the mean of logarithm of 50% growth inhibition (GI_{50}) (MG-MID) values of *s*-triazine derivatives. A high and statistically significant correlation (r = .98, Pearson correlation coefficient, and P = .023) was observed between the two activities (n = 4). All statistical tests were two-sided.

Correlation of PI3K Inhibition with Growth-Inhibitory Activity of *s*-Triazine Derivatives

ZSTK474 is an *s*-triazine derivative, as are ZSTK1178, ZSTK781, and ZSTK116, and all have different PI3K inhibitory activities. We investigated whether the PI3K inhibitory activities (IC_{50}) of these four *s*-triazine derivatives were related to their growth inhibitory activities (assessed as the mean logarithm of GI_{50}). A statistically significantly high correlation (r = .98 and P = .023) was observed between these two inhibitory activities (Fig. 3, C), suggesting that ZSTK474 inhibited cell proliferation by inhibiting PI3K activity.

Molecular Modeling of the PI3K–ZSTK474 Complex

Because all previously described PI3K inhibitors apparently bind to the ATP-binding site of p110, the catalytic subunit of PI3K *(44)*, we investigated whether ZSTK474 also binds to this site by using a model structure, the crystal structure of the PI3Kγ–LY294002 complex, to generate a PI3K template structure for docking analysis *(44)*. Analysis of this model structure indicated that there are three hydrogen-bonding interactions between PI3K and ZSTK474 (i.e., K802 NZ, one of the morpholino oxygens; S806 OG, the other morpholino oxygen; and V882 NH, the benzimidazole nitrogen [Fig. 4, A]).

We next compared the binding modes of ZSTK474 with those of ATP in the active site of PI3K. Two of the three hydrogen bonds between ZSTK474 and PI3K, V882 NH and S806 OG, mimicked those in the ATP–PI3K complex; therefore, the overall arrangements of ZSTK474 and ATP in the PI3K active site are very close (Fig. 4, B). The benzimidazole nitrogen of ZSTK474 forms a hydrogen bond with V882 NH. This hydrogen bond mimics the hydrogen bond between ATP N1 and V882 NH. As discussed previously *(45)*, all kinase inhibitors appear to have a hydrogen bond acceptor in a position equivalent to ATP N1. These features of the ZSTK474–PI3K complex support the hypothesis that ZSTK474 binds to the ATP-binding site of PI3K. In contrast, ZSTK474 and LY294002 appear to bind to different sites in the ATP-binding pocket (Fig. 4, C), with LY294002 forming two hydrogen bonds between PI3K at V882 NH and K833 NZ.

As shown in Fig. 4, D and E, the amino acid residues Met-804 (M804), Trp-812 (W812), and Met-953 (M953) of PI3K create a unique space in the ATP-binding pocket that is larger than the

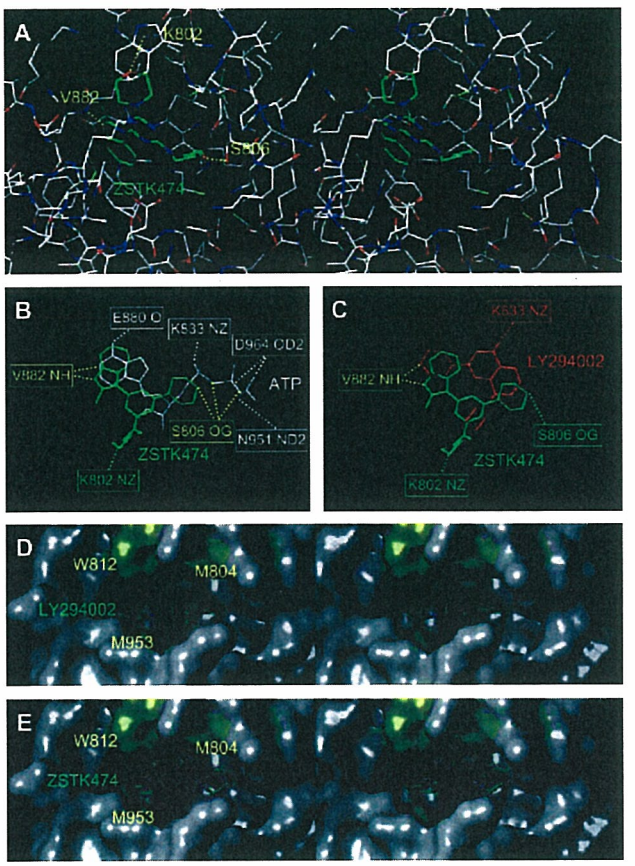

Fig. 4. Molecular modeling of the PI3K–ZSTK474 complex. A) Stereo view of the model structure of the PI3K–ZSTK474 complex. Putative hydrogen bonds = **yellow dashed lines**. Carbon atoms of PI3K = **white**; nitrogens = **blue**; oxygens = **red**. B and C) Binding modes in the PI3K active site. B) Comparison of ZSTK474 and ATP. ZSTK474 = **green**; ATP = **white**. C) Comparison of ZSTK474 and LY294002. ZSTK474 = **green**; LY294002 = **red**. D and E) Stereoview of the interactions between PI3K amino acid residues (M804, W812, and M953) and LY204002 or ZSTK474. D) LY294002 and PI3K. Amino acid residues = **yellow**; LY294002 = **green**. E) ZSTK474 and PI3K. Amino acid residues = **yellow**; ZSTK474 = **green**.

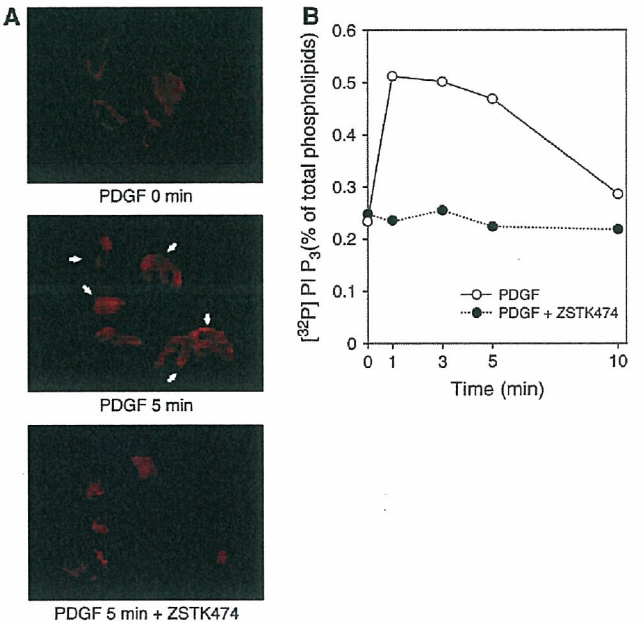

Fig. 5. Effect of ZSTK474 on membrane ruffling and the formation of phosphatidylinositol-3,4,5-trisphosphate (PIP_3). A) Inhibition of membrane ruffling in murine embryonic fibroblasts (MEFs) by ZSTK474. MEFs were treated with or without 1 μM ZSTK474 for 15 minutes and then stimulated with platelet-derived growth factor (10 ng/mL) for 5 minutes. Cells were then fixed and stained for filamentous actin with tetramethylrhodamine isothiocyanate–conjugated phalloidin (**red**). **Arrows** indicate cells with membrane ruffling. B) Inhibition of PIP_3 formation by ZSTK474. MEFs were labeled with [^{32}P]orthophosphate (0.1 mCi/mL) for 4 hours, treated with or without 1 μM ZSTK474 for 15 minutes, and then stimulated with platelet-derived growth factor (10 ng/mL) as indicated. Radioactivity in the total phospholipids and in PIP_3 was determined with a bioimaging analyzer. Data are the percentage of radioactive PIP_3 as a function of radioactivity in total lipids.

corresponding portion of the ATP-binding pocket of other protein kinases *(44)*. In our models, this space was occupied by the bulky 8-phenyl group of LY294002 (Fig. 4, D), as previously indicated by Walker et al. *(44)*, or by the triazine and morpholino groups of ZSTK474 (Fig. 4, E).

Inhibition of Membrane Ruffling by ZSTK474

It is widely accepted that membrane ruffling is regulated by PI3K by means of a pathway that is independent of Akt, a serine/threonine protein kinase. We examined ZSTK474 for its effect on membrane ruffling induced by platelet-derived growth factor in murine embryonic fibroblast cells. We found that membrane ruffling was induced 5 minutes after platelet-derived growth factor was added to the cultures (Fig. 5, A). When cells were incubated for 15 minutes with 1 μM ZSTK474 before the addition of platelet-derived growth factor, both membrane ruffling and the formation of PIP_3, a measure of PI3K activity, were blocked (Fig. 5, B). Thus, ZSTK474 appears to inhibit PI3K activity and also to block membrane ruffling.

Effects of ZSTK474 on Apoptosis and Cell Cycle

Because PI3K and its downstream components appear to mediate antiapoptotic signals, we examined the effect of ZSTK474 on the induction of apoptosis. At 10 μM, a higher concentration than its GI_{50}, ZSTK474 induced apoptosis in OVCAR3 cells (Fig. 6, A and B). However, 10 μM ZSTK474 did not induce apoptosis in A549 cells but instead mediated complete G_1-phase arrest (Fig. 6, C). Therefore, it appears that induction of apoptosis by ZSTK474 is a weak and cell type-dependent event. Here the induction of G_1-phase arrest by ZSTK474 might lead to the inhibition of tumor growth in vivo, which was indeed observed in the animal experiments with A549 below.

Inhibition of Akt Phosphorylation and Downstream Signaling by ZSTK474

The time course of ZSTK474-mediated inhibition of the phosphorylation of Akt, one of the major targets of PI3K, and inhibition of other downstream signaling components was examined in A549 cells by immunoblotting. Treatment with 0.5 μM ZSTK474 decreased the level of phosphorylated Akt (Ser-473) within 5 minutes without altering overall Akt protein levels and then decreased the level of phosphorylated GSK-3β (Ser-9) and of cyclin D1 protein expression within 30 minutes (Fig. 7, A). We next investigated the effect of various concentrations of ZSTK474

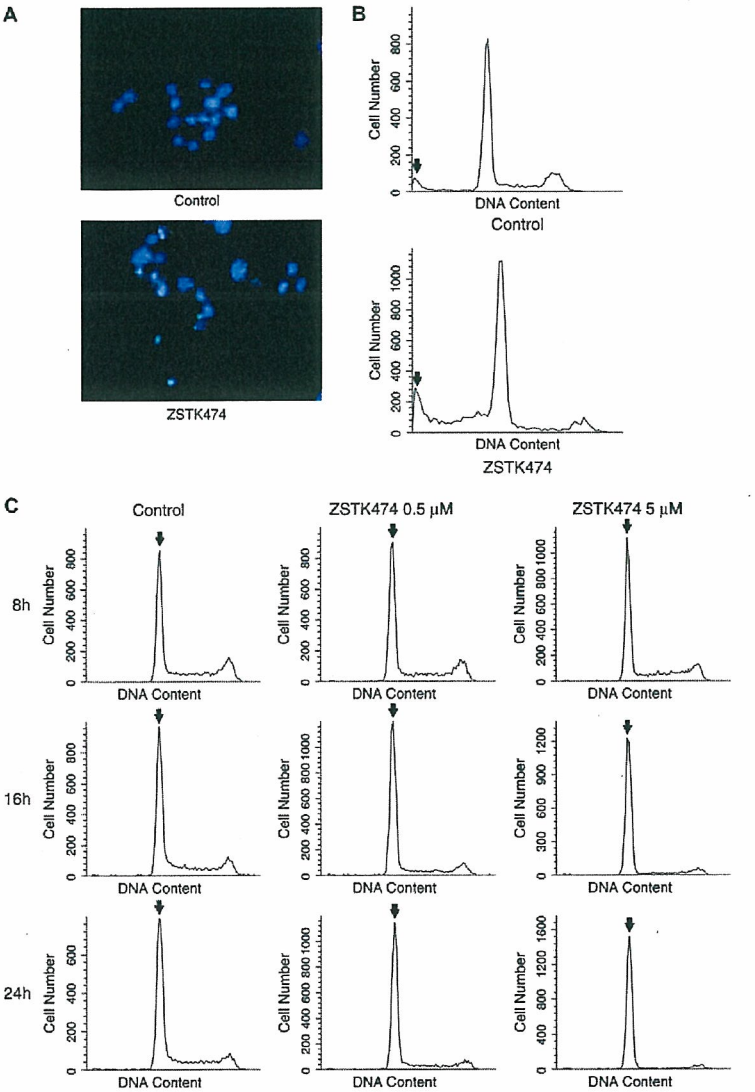

Fig. 6. Effects of ZSTK474 on apoptosis and cell cycle. **A)** Apoptosis assessed by chromatin condensation. OVCAR3 cells were cultured in RPMI 1640 medium supplemented with 5% fetal bovine serum for 24 hours and then cultured for 48 hours with or without 10 μM ZSTK474. Cells were stained with Hoechst 33342 and examined by fluorescence microscopy. Morphologic changes induced by ZSTK474, such as the condensation of chromatin, were indicative of apoptosis. **B)** Apoptosis as assessed by flow cytometry. OVCAR3 cells cultured under the same conditions as in **panel A** were harvested, washed with ice-cold phosphate-buffered saline (PBS), and fixed in 70% ethanol. Cells were then washed twice with ice-cold PBS again, treated with RNase A (500 μg/mL, Sigma) at 37 °C for 1 hour, and stained with propidium iodide (25 μg/mL, Sigma). The DNA content of the cells was analyzed with a flow cytometer (FACScalibur, Becton Dickinson). When exposed to ZSTK474, the sub-G_1 peak increased, indicating that ZSTK474 induced apoptosis. **Arrows** indicate the sub-G1 peaks. **C)** Cell cycle analysis as assessed by flow cytometry. A549 cells were exposed to 0.5 or 5 μM ZSTK474 for 8, 16, or 24 hours. The DNA content of the cells was determined by flow cytometry as described above. When exposed to ZSTK474, the cell population in G_1 phase increased time dependently, indicating that ZSTK474 blocked the cell cycle at the G_1 phase. **Arrows** indicate the G_1 peaks.

from 0 to 2.0 μM on the levels of downstream signaling components in the Akt pathway. ZSTK474 inhibited the phosphorylation of forkhead in rhabdomyosarcoma-like 1 (FKHRL1) on Thr-32, forkhead in rhabdomyosarcoma (FKHR) on Thr-24, tuberous sclerosis complex 2 (TSC-2) on Ser-1462, mammalian target of rapamycin (mTOR) on Ser-2448, and p70 ribosomal protein S6 kinase (p70S6K) on Thr-389 and decreased the expression of cyclin D1 protein in a dose–dependent manner (Fig. 7, B). In contrast, phosphorylation of extracellular signal-regulated kinases (ERK1/2) and mitogen-activated protein kinase/extracellular signal–regulated kinase kinases (MEK1/2) were not inhibited by ZSTK474, suggesting that ZSTK474 did not inhibit the RAS–ERK pathway (Fig. 7, A and B). Thus ZSTK474 also appears to act through the Akt pathway.

Antitumor Efficacy of ZSTK474 In Vivo

We evaluated the antitumor activity and toxicity of ZSTK474 by use of a mouse cancer model and three human cancer xenograft models. When administered orally for 2 weeks, ZSTK474 inhibited the growth of subcutaneously implanted mouse B16F10 melanoma tumors in a dose-dependent manner. Almost complete tumor growth inhibition (i.e., tumor regression) was observed at higher dosages. Administration of ZSTK474 at 100, 200, or 400 mg/kg produced tumor regression of 28.5% (95% CI = 21.4% to 35.7%), 7.1% (95% CI = 2.7% to 11.5%), or 4.9% (95% CI = 3.2% to 6.5%) on day 14, respectively. This growth inhibition was superior to that of the four major anticancer drugs examined—irinotecan, cisplatin, doxorubicin, and 5-fluorouracil (each administered at their respective maximum tolerable doses). Tumor regression in mice of treated with irinotecan, cisplatin, doxorubicin, or 5-fluorouracil was 96.0% (95% CI = 63.5% to 128.4%), 35.7% (95% CI = 28.6% to 42.9%), 24.0% (95% CI = 16.4% to 31.5%), or 68.3% (95% CI = 21.4% to 115.3%) on day 14, respectively (Fig. 8, A). Moreover, the myelosuppression induced by ZSTK474 at 400 mg/kg was marginal (Fig. 8, B).

We then examined the antitumor activity of ZSTK474 against A549, PC-3, and WiDr human xenografts, which originated from a non–small-cell lung cancer, a prostate cancer, and a colon cancer, respectively. Chronic oral administration of ZSTK474 completely

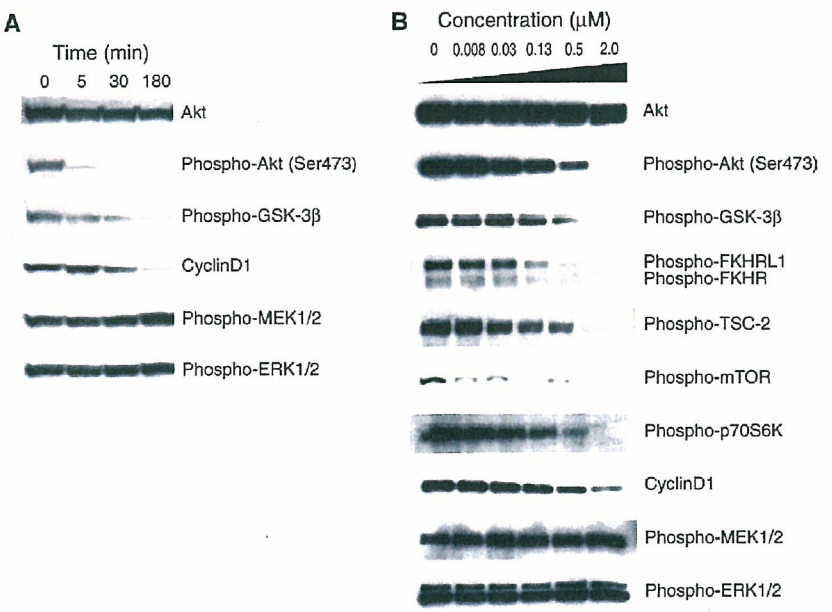

Fig. 7. Immunoblot analysis of Akt and downstream components in the Akt pathway in ZSTK474-treated cells. A) Time course. A549 cells were treated with 0.5 μM ZSTK474 as indicated. B) Inhibition as a function of ZSTK474 concentration. A549 cells were treated with the concentration of ZSTK474 indicated for 3 hours. After treatment with ZSTK474, cells were harvested for immunoblot analysis with antibodies specific for nonphosphorylated or phosphorylated proteins indicated of Akt phosphorylation, the level of cyclin D1, and the phosphorylation of downstream components, including glycogen synthase kinase 3β (GSK-3β), extracellular signal–regulated kinases (ERK1/2), mitogen-activated protein kinase/extracellular signal–regulated kinase kinases (MEK1/2), forkhead in rhabdomyosarcoma-like 1 (FKHRL1), forkhead in rhabdomyosarcoma (FKHR), tuberous sclerosis complex 2 (TSC-2), mammalian target of rapamycin (mTOR), and p70 ribosomal protein S6 kinase (p70S6K).

inhibited growth of A549, PC-3, and WiDr xenografts at a dose of 400 mg/kg (Fig. 8, C [upper panels] and D), and it induced the regression of A549 xenograft tumors. To assess toxicity, we measured the body weight of the tumor-bearing mice. Their weight was slightly reduced by administration of ZSTK474, but the reduction was tolerable (no reduction, 17% reduction, and 3% reduction of the day 0 weight on day 14 in A549-bearing mice, in PC-3-bearing mice, in WiDr-bearing mice, respectively) (Fig. 8, C [lower panels]). Dermal toxicity has been reported when LY294002 administered to nude mice *(46)*. However, we observed no dermal toxicity with ZSTK474 even after more than 28 days, as shown in Fig. 8, D. Furthermore, chronic oral administration of ZSTK474 at a higher dose (800 mg/kg) over 4 weeks again reduced body weight within a tolerable range (14% reduction of the day 0 weight on day 28), without toxic effects in critical organs. Thus ZSTK474 appeared to have good therapeutic efficacy in vivo.

Inhibition of the Phosphorylation of Akt by ZSTK474 In Vivo

To confirm that ZSTK474 inhibits the PI3K pathway in vivo, the phosphorylation status of Akt in the subcutaneous A549 tumor tissue was immunohistochemically determined by an anti-Akt antibody specific for phosphorylation at Akt amino acid residue Ser-473. We found that administration of ZSTK474 reduced the level of Akt phosphorylation in tumor tissue (Fig. 8, E).

Discussion

In this study, we demonstrated that a new compound, ZSTK474, is a potent inhibitor of PI3K that differs structurally from the well-known PI3K inhibitors LY294002 and wortmannin. We also demonstrated that orally administered ZSTK474 has therapeutic efficacy against human cancer xenografts in mice. To the best of our knowledge, this is the first report of an orally administered PI3K inhibitor that has strong antitumor activity without severe toxicity in vivo. The PI3K pathway is activated in various cancer types, and therefore PI3K is a promising therapeutic target of cancer *(3,4,21)*. Thus ZSTK474 appears to be a new anticancer drug candidate targeting PI3K.

From a methodology viewpoint, another novelty of this study is our use of an information-intensive approach, COMPARE analysis, to identify the target of ZSTK474. The COMPARE analysis predicted that the target of ZSTK474 was PI3K, which was later confirmed by direct inhibition of PI3K activity with ZSTK474. We have previously identified the targets of new compounds MS-247 *(26)* and FJ5002 *(47)* as topoisomerase I/II and telomerase, respectively, by using COMPARE analysis. This study further confirms that the COMPARE analysis is a powerful tool that can predict the molecular targets of new compounds.

Molecular modeling of the PI3K–ZSTK474 complex indicated that ZSTK474 could bind to the ATP-binding pocket of PI3K through three hydrogen bonds, which is a finding consistent with the ZSTK474-mediated inhibition of PI3K being reversible. Because ZSTK474 formed three hydrogen bonds with PI3K, instead of the two hydrogen bonds formed between LY294002 and PI3K, ZSTK474 appears to be a stronger competitor for the ATP-binding pocket of PI3K than LY294002. Indeed, the PI3K inhibitory activity of ZSTK474 was approximately 20-fold stronger than that of LY294002. Another important feature of ZSTK474 is its high specificity for PI3K. When tested at 30 μM, ZSTK474 did not inhibit the activity of 139 other

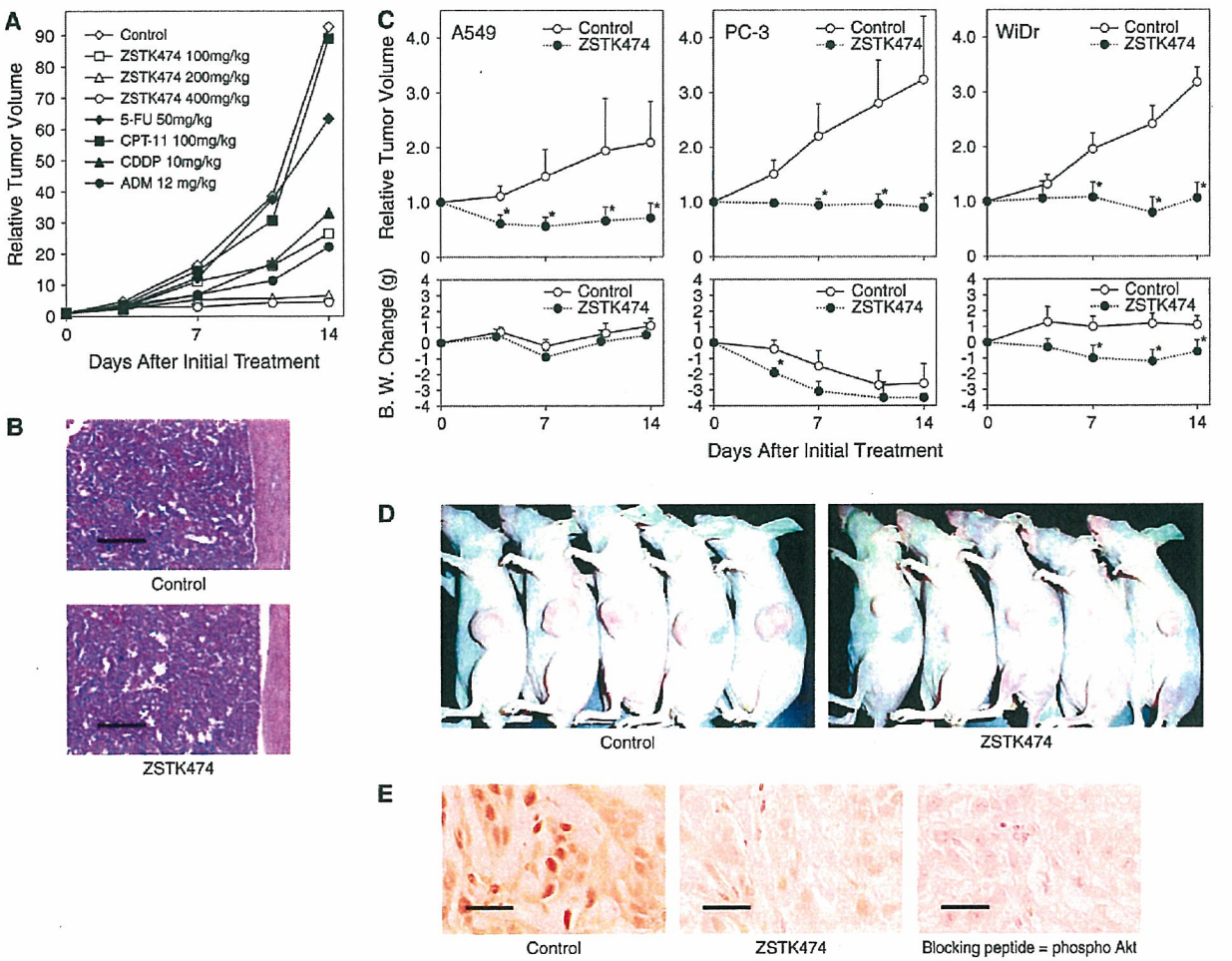

Fig. 8. Antitumor activity of ZSTK474. A) Antitumor activity of ZSTK474 against mouse B16F10 melanomas. Fifty-six BDF_1 mice were each subcutaneously injected with 5×10^5 B16F10 melanoma tumor cells. Seven days after inoculation, the administration of the drugs, as indicated, began (day 0). ZSTK474 was orally administered daily from days 0 to 13. Reference drugs were irinotecan (CPT-11), cisplatin (CDDP), doxorubicin (ADM), and 5-fluorouracil (5-FU). Each reference drug was administered intravenously from day 0 at the maximum tolerable dose by use of the following optimal schedules: CPT-11 at 100 mg/kg administered three times on days 0, 3, and 7; CDDP at 10 mg/kg once on day 0; ADM at 12 mg/kg once on day 0; and 5-FU at 50 mg/kg three times on days 0, 3, and 7. Each data point is the average of data from seven mice. **B)** Hematoxylin–eosin staining of femur bone marrow sections from BDF_1 mice bearing B16F10 melanomas 14 days after inoculation of tumor cells. ZSTK474 at 400 mg/kg was orally administered daily from days 0 to13. **Scale bar** = 100 μm. **C)** ZSTK474 and tumor growth and body weight in nude mice bearing human cancer xenografts. Forty-five nude mice were subcutaneously inoculated with a tumor fragment of 3 mm × 3 mm × 3 mm from the subcutaneous tumor developed in nude mice. When tumors reached a volume of 100–300 mm^3, animals were divided randomly into test groups, each with five mice (day 0). ZSTK474 (400 mg/kg) was orally administered daily from day 0 to 13 except for days 3 and 10. Data are the means of data from five mice. **Error bar** = the upper 95% confidence interval. *P = .009, two-sided Mann–Whitney U test, compared with respective control. **D)** WiDr xenograft growth inhibition after administration of ZSTK474. ZSTK474 at 400 mg/kg was orally administered daily from days 0 to 26, except for days 6, 13, and 20. The mice were photographed on day 28. Other experimental conditions were the same as described above. **E)** ZSTK474 and Akt phosphorylation in nude mice bearing A549 human non–small-cell lung cancer xenografts. When the volume of tumors reached 100–300 mm^3, ZSTK474 at 400 mg/kg was orally administered once. Mice were killed 4 hours after ZSTK474 administration, and excised tumors were analyzed by immunohistochemistry for the expression of phosphorylated Akt (Ser-473). Phosphorylated Akt (Ser-473) blocking peptide was incubated with phosphorylated Akt (Ser-473) antibody at 4 °C for 2 hours before incubating with the tissue section. **Scale bar** = 25 μm.

protein kinases examined. The three-dimensional space in the ATP-binding pocket of PI3K is larger than the corresponding spaces found in the ATP-binding pockets of other protein kinases *(44)*. The triazine and morpholino groups of ZSTK474 fit well into this space. Therefore, these moieties may be important in the specificity of ZSTK474 for PI3K. To further confirm the binding of ZSTK474 to the ATP-binding pocket of PI3K, a biochemical experiment that examines whether ZSTK474 competitively inhibits the binding of ATP to its binding site is required.

PI3K plays an important role in the proliferation of tumor cells. We compared ZSTK474 with other PI3K inhibitors, LY294002 and wortmannin, for its ability to inhibit cell proliferation. At concentrations of less than 1 μM, ZSTK474 potently inhibited the growth of various cancer cell lines. The growth inhibitory activity of ZSTK474 was more than 10-fold stronger than that of wortmannin, which may be due to wortmannin's being somewhat unstable in cell culture medium *(48)*, or of LY294002, which may be due to the PI3K inhibitory activity of LY294002 being more than 10-fold weaker than that of ZSTK474. Furthermore, the PI3K inhibitory activities of other *s*-triazine derivatives statistically significantly correlated with their cell growth inhibitory activities. These results suggested that ZSTK474 inhibited cell

growth by inhibiting PI3K, with subsequent inhibitory effects on downstream signaling molecules.

PI3K participates in the induction of the membrane ruffling. ZSTK474 inhibited platelet-derived growth factor–induced membrane ruffling in murine embryonic fibroblast cells, which is an Akt-independent process, and inhibited the generation of PIP_3. These results demonstrate that ZSTK474 inhibited PI3K activity in intact cells.

Because the PI3K pathway is considered to mediate antiapoptotic signals in tumor cells, ZSTK474 was expected to induce apoptosis efficiently by inhibiting PI3K. However, we observed weak or no induction of apoptosis after ZSTK474 treatment in OVCAR3 cells or A549 cells, respectively. Therefore, induction of apoptosis by ZSTK474 appears to be a cell type–dependent event, probably because of the differential status of the PI3K signaling pathway in various cancer cell lines.

One of the major downstream effectors of PI3K is Akt, a serine/threonine protein kinase. Therefore, we investigated the effect of PI3K on the activation of Akt and its key downstream components. ZSTK474 reduced, in a time-dependent manner, phosphorylation of the protein kinases Akt and GSK-3β and the expression of cyclin D1 protein. Akt inhibits cyclin D1 degradation by regulating the activity of GSK-3β *(49)*. After its phosphorylation by GSK-3β, cyclin D1 is targeted for degradation by the proteasome. Akt phosphorylates GSK-3β directly and blocks its kinase activity, thereby allowing cyclin D1 to accumulate in cells *(49)*. ZSTK474 inhibited the phosphorylation of other downstream signaling components that are involved in regulating cell proliferation (i.e., FKHRL1, FKHR, TSC-2, mTOR, and p70S6K) in a dose-dependent manner. These results indicated that the inhibition of PI3K by ZSTK474 was followed by a decrease in relevant downstream signaling, which may in turn facilitate cell growth inhibition. In fact, we observed complete G_1-phase arrest in A549 cells after ZSTK474 treatment. In contrast, ZSTK474 did not inhibit phosphorylation of either ERK1/2 or MEK1/2, suggesting that ZSTK474 does not inhibit components in the RAS–ERK pathway.

Orally administered ZSTK474 displayed potent antitumor activity against human cancer xenografts in mice, without evidence of critical toxicity. Known PI3K inhibitors—such as LY294002 *(46,50–52)*, wortmannin *(53,54)*, and viridin analogues *(54)*—have previously been examined for their antitumor activities. In most reports, LY294002, which was administered intraperitoneally because it is insoluble in water, had antitumor activity when administered at an early stage (i.e., within 7 days after inoculation of tumor cells) *(50)*, but it also induced severe dermal toxicity *(46)*. Wortmannin also had antitumor activity, but again it achieved sufficient efficacy only when administered at an early stage *(53)*, and it caused liver toxicity *(54)*. An analogue of wortmannin, PX-866, has recently been developed *(54)* that has better efficacy and lower toxicity than wortmannin. However, this agent still produces liver toxicity *(54)*. In this study, we found that ZSTK474 had strong antitumor efficacy against advanced-stage tumors (i.e., >15 days after inoculation of tumor cells) and that ZSTK474 did not produce noticeable toxicity in critical organs after daily administration for more than 14 days. We also confirmed reduction of Akt phosphorylation after ZSTK474 administration. Thus, the reduction of Akt phosphorylation may be a useful biomarker marker to monitor the efficacy of ZSTK474 in future investigations of ZSTK474.

Although ZSTK474 indicated favorable features for a novel anticancer drug candidate as described above, various preclinical studies remain before ZSTK474 can be evaluated in a clinical trial, which include more precise investigation of the molecular pharmacology, analyses of the pharmacokinetics and the pharmacodynamics, and careful investigation of the toxicity. Investigation of the toxicity derived from PI3K inhibition is especially important because PI3K is expressed in various normal tissues. These studies are currently under way.

In conclusion, we demonstrated that the compound ZSTK474 is a new PI3K inhibitor and that it has strong antitumor activity against human cancer xenografts without critical toxicity. It appears that ZSTK474 can be orally administered over long periods, which may be important for the treatment of cancer. Thus, ZSTK474 merits further investigation as an anticancer drug.

References

(1) Auger KR, Serunian LA, Soltoff SP, Libby P, Cantley LC. PDGF-dependent tyrosine phosphorylation stimulates production of novel polyphosphoinositides in intact cells. Cell 1989;57:167–75.

(2) Whitman M, Downes CP, Keeler M, Keller T, Cantley L. Type I phosphatidylinositol kinase makes a novel inositol phospholipid, phosphatidylinositol-3-phosphate. Nature 1988;332:644–6.

(3) Vivanco I, Sawyers CL. The phosphatidylinositol 3-Kinase AKT pathway in human cancer. Nat Rev Cancer 2002;2:489–501.

(4) Luo J, Manning BD, Cantley LC. Targeting the PI3K-Akt pathway in human cancer: rationale and promise. Cancer Cell 2003;4:257–62.

(5) Aoki M, Schetter C, Himly M, Batista O, Chang HW, Vogt PK. The catalytic subunit of phosphoinositide 3-kinase: requirements for oncogenicity. J Biol Chem 2000;275:6267–75.

(6) Jimenez C, Jones DR, Rodriguez-Viciana P, Gonzalez-Garcia A, Leonardo E, Wennstrom S, et al. Identification and characterization of a new oncogene derived from the regulatory subunit of phosphoinositide 3-kinase. EMBO J 1998;17:743–53.

(7) Samuels Y, Wang Z, Bardelli A, Silliman N, Ptak J, Szabo S, et al. High frequency of mutations of the PIK3CA gene in human cancers. Science 2004;304:554.

(8) Levine DA, Bogomolniy F, Yee CJ, Lash A, Barakat RR, Borgen PI, et al. Frequent mutation of the PIK3CA gene in ovarian and breast cancers. Clin Cancer Res 2005;11:2875–8.

(9) Shayesteh L, Lu Y, Kuo WL, Baldocchi R, Godfrey T, Collins C, et al. PIK-3CA is implicated as an oncogene in ovarian cancer. Nat Genet 1999;21: 99–102.

(10) Pedrero JM, Carracedo DG, Pinto CM, Zapatero AH, Rodrigo JP, Nieto CS, et al. Frequent genetic and biochemical alterations of the PI 3-K/AKT/PTEN pathway in head and neck squamous cell carcinoma. Int J Cancer 2005;114:242–8.

(11) Kobayashi M, Nagata S, Iwasaki T, Yanagihara K, Saitoh I, Karouji Y, et al. Dedifferentiation of adenocarcinomas by activation of phosphatidylinositol 3-kinase. Proc Natl Acad Sci U S A 1999;96:4874–9.

(12) Steck PA, Pershouse MA, Jasser SA, Yung WK, Lin H, Ligon AH, et al. Identification of a candidate tumour suppressor gene, MMAC1, at chromosome 10q23.3 that is mutated in multiple advanced cancers. Nat Genet 1997;15:356–62.

(13) Lee HY, Srinivas H, Xia D, Lu Y, Superty R, LaPushin R, et al. Evidence that phosphatidylinositol 3-kinase- and mitogen-activated protein kinase kinase-4/c-Jun NH2-terminal kinase-dependent Pathways cooperate to maintain lung cancer cell survival. J Biol Chem 2003;278:23630–8.

(14) Czauderna F, Fechtner M, Aygun H, Arnold W, Klippel A, Giese K, et al. Functional studies of the PI*(3)*-kinase signalling pathway employing synthetic and expressed siRNA. Nucleic Acids Res 2003;31:670–82.

(15) Okada T, Sakuma L, Fukui Y, Hazeki O, Ui M. Blockage of chemotactic peptide-induced stimulation of neutrophils by wortmannin as a result of selective inhibition of phosphatidylinositol 3-kinase. J Biol Chem 1994;269:3563–7.

(16) Powis G, Bonjouklian R, Berggren MM, Gallegos A, Abraham R, Ashendel C, et al. Wortmannin, a potent and selective inhibitor of phosphatidylinositol-3-kinase. Cancer Res 1994;54:2419–23.

(17) Wipf P, Minion DJ, Halter RJ, Berggren MI, Ho CB, Chiang GG, et al. Synthesis and biological evaluation of synthetic viridins derived from C(20)-heteroalkylation of the steroidal PI-3-kinase inhibitor wortmannin. Org Biomol Chem 2004;2:1911–20.
(18) Woscholski R, Kodaki T, McKinnon M, Waterfield MD, Parker PJ. A comparison of demethoxyviridin and wortmannin as inhibitors of phosphatidylinositol 3-kinase. FEBS Lett 1994;342:109–14.
(19) Vlahos CJ, Matter WF, Hui KY, Brown RF. A specific inhibitor of phosphatidylinositol 3-kinase, 2-(4-morpholinyl)-8-phenyl-4H-1-benzopyran-4-one (LY294002). J Biol Chem 1994;269:5241–8.
(20) West KA, Castillo SS, Dennis PA. Activation of the PI3K/Akt pathway and chemotherapeutic resistance. Drug Resist Updat 2002;5:234–48.
(21) Workman P. Inhibiting the phosphoinositide 3-kinase pathway for cancer treatment. Biochem Soc Trans 2004;32:393–6.
(22) Yaguchi S, Izumisawa Y, Sato M, Nakagane T, Koshimizu I, Sakita K, et al. In vitro cytotoxicity of imidazolyl-1,3,5-triazine derivatives. Biol Pharm Bull 1997;20:698–700.
(23) Matsuno T, Karo M, Sasahara H, Watanabe T, Inaba M, Takahashi M, et al. Synthesis and antitumor activity of benzimidazolyl-1,3,5-triazine and benzimidazolylpyrimidine derivatives. Chem Pharm Bull (Tokyo) 2000;48:1778–81.
(24) Dan S, Tsunoda T, Kitahara O, Yanagawa R, Zembutsu H, Katagiri T, et al. An integrated database of chemosensitivity to 55 anticancer drugs and gene expression profiles of 39 human cancer cell lines. Cancer Res 2002;62: 1139–47.
(25) Yamori T. Panel of human cancer cell lines provides valuable database for drug discovery and bioinformatics. Cancer Chemother Pharmacol 2003; 52 Suppl 1:S74–9.
(26) Yamori T, Matsunaga A, Sato S, Yamazaki K, Komi A, Ishizu K, et al. Potent antitumor activity of MS-247, a novel DNA minor groove binder, evaluated by an in vitro and in vivo human cancer cell line panel. Cancer Res 1999;59:4042–9.
(27) Monks A, Scudiero D, Skehan P, Shoemaker R, Paull K, Vistica D, et al. Feasibility of a high-flux anticancer drug screen using a diverse panel of cultured human tumor cell lines. J Natl Cancer Inst 1991;83:757–66.
(28) Paull KD, Shoemaker RH, Hodes L, Monks A, Scudiero DA, Rubinstein L, et al. Display and analysis of patterns of differential activity of drugs against human tumor cell lines: development of mean graph and COMPARE algorithm. J Natl Cancer Inst 1989;81:1088–92.
(29) Fidler IJ. Biological behavior of malignant melanoma cells correlated to their survival in vivo. Cancer Res 1975;35:218–24.
(30) Skehan P, Storeng R, Scudiero D, Monks A, McMahon J, Vistica D, et al. New colorimetric cytotoxicity assay for anticancer-drug screening. J Natl Cancer Inst 1990;82:1107–12.
(31) Boyd MR. Status of the National Cancer Institute preclinical antitumor drug discovery screen: implications for selection of new agents for clinical trial. Vol 3. Philadelphia (PA): Lippincott; 1989.
(32) Fukui Y, Kornbluth S, Jong SM, Wang LH, Hanafusa H. Phosphatidylinositol kinase type I activity associates with various oncogene products. Oncogene Res 1989;4:283–92.
(33) Gray A, Olsson H, Batty IH, Priganica L, Peter Downes C. Nonradioactive methods for the assay of phosphoinositide 3-kinases and phosphoinositide phosphatases and selective detection of signaling lipids in cell and tissue extracts. Anal Biochem 2003;313:234–45.
(34) Rarey M, Kramer B, Lengauer T, Klebe G. A fast flexible docking method using an incremental construction algorithm. J Mol Biol 1996;261:470–89.
(35) Tsujishita H, Hirono S. CAMDAS: an automated conformational analysis system using molecular dynamics. Conformational Analyzer with Molecular Dynamics And Sampling. J Comput Aided Mol Des 1997;11:305–15.
(36) Radwan AA, Gouda H, Yamaotsu N, Torigoe H, Hirono S. Rational procedure for 3D-QSAR analysis using TRNOE experiments and computational methods: application to thermolysin inhibitors. Drug Des Discov 2001;17:265–81.
(37) Kuntz ID, Blaney JM, Oatley SJ, Langridge R, Ferrin TE. A geometric approach to macromolecule-ligand interactions. J Mol Biol 1982;161:269–88.
(38) Jones G, Willett P, Glen RC, Leach AR, Taylor R. Development and validation of a genetic algorithm for flexible docking. J Mol Biol 1997;267: 727–48.
(39) Eldridge MD, Murray CW, Auton TR, Paolini GV, Mee RP. Empirical scoring functions: I. The development of a fast empirical scoring function to estimate the binding affinity of ligands in receptor complexes. J Comput Aided Mol Des 1997;11:425–45.
(40) Muegge I, Martin YC. A general and fast scoring function for protein-ligand interactions: a simplified potential approach. J Med Chem 1999;42:791–804.
(41) Katsuki M, Chuang VT, Nishi K, Kawahara K, Nakayama H, Yamaotsu N, et al. Use of photoaffinity labeling and site-directed mutagenesis for identification of the key residue responsible for extraordinarily high affinity binding of UCN-01 in human alpha1-acid glycoprotein. J Biol Chem 2005;280:1384–91.
(42) Kimura K, Hattori S, Kabuyama Y, Shizawa Y, Takayanagi J, Nakamura S, et al. Neurite outgrowth of PC12 cells is suppressed by wortmannin, a specific inhibitor of phosphatidylinositol 3-kinase. J Biol Chem 1994;269:18961–7.
(43) Plank J, Rychlo A. [A method for quick decalcification.]. Zentralbl Allg Pathol 1952;89:252–4.
(44) Walker EH, Pacold ME, Perisic O, Stephens L, Hawkins PT, Wymann MP, et al. Structural determinants of phosphoinositide 3-kinase inhibition by wortmannin, LY294002, quercetin, myricetin, and staurosporine. Mol Cell 2000;6:909–19.
(45) Lawrie AM, Noble ME, Tunnah P, Brown NR, Johnson LN, Endicott JA. Protein kinase inhibition by staurosporine revealed in details of the molecular interaction with CDK2. Nat Struct Biol 1997;4:796–801.
(46) Hu L, Zaloudek C, Mills GB, Gray J, Jaffe RB. In vivo and in vitro ovarian carcinoma growth inhibition by a phosphatidylinositol 3-kinase inhibitor (LY294002). Clin Cancer Res 2000;6:880–6.
(47) Naasani I, Seimiya H, Yamori T, Tsuruo T. FJ5002: a potent telomerase inhibitor identified by exploiting the disease-oriented screening program with COMPARE analysis. Cancer Res 1999;59:4004–11.
(48) Holleran JL, Egorin MJ, Zuhowski EG, Parise RA, Musser SM, Pan SS. Use of high-performance liquid chromatography to characterize the rapid decomposition of wortmannin in tissue culture media. Anal Biochem 2003;323:19–25.
(49) Diehl JA, Cheng M, Roussel MF, Sherr CJ. Glycogen synthase kinase-3beta regulates cyclin D1 proteolysis and subcellular localization. Genes Dev 1998;12:3499–511.
(50) Su JD, Mayo LD, Donner DB, Durden DL. PTEN and phosphatidylinositol 3′-kinase inhibitors up-regulate p53 and block tumor-induced angiogenesis: evidence for an effect on the tumor and endothelial compartment. Cancer Res 2003;63:3585–92.
(51) Semba S, Itoh N, Ito M, Harada M, Yamakawa M. The in vitro and in vivo effects of 2-(4-morpholinyl)-8-phenyl-chromone (LY294002), a specific inhibitor of phosphatidylinositol 3′-kinase, in human colon cancer cells. Clin Cancer Res 2002;8:1957–63.
(52) Bondar VM, Sweeney-Gotsch B, Andreeff M, Mills GB, McConkey DJ. Inhibition of the phosphatidylinositol 3′-kinase-AKT pathway induces apoptosis in pancreatic carcinoma cells in vitro and in vivo. Mol Cancer Ther 2002;1:989–97.
(53) Lemke LE, Paine-Murrieta GD, Taylor CW, Powis G. Wortmannin inhibits the growth of mammary tumors despite the existence of a novel wortmannin-insensitive phosphatidylinositol-3-kinase. Cancer Chemother Pharmacol 1999;44:491–7.
(54) Ihle NT, Williams R, Chow S, Chew W, Berggren MI, Paine-Murrieta G, et al. Molecular pharmacology and antitumor activity of PX-866, a novel inhibitor of phosphoinositide-3-kinase signaling. Mol Cancer Ther 2004;3:763–72.

NOTES

We thank Dr. R. H. Shoemaker and Dr. K. D. Paull for discussion on the establishment of JFCR39 and COMPARE analysis; Ms. Y. Nishimura, Ms. M. Seki, Ms. Y. Mukai, Ms. M. Okamura, and Dr. Y. Yoshida for technical assistance; Mr. T. Watanabe, Dr. Y. Tsuchida and Mr. K. Saito for synthesis of compounds; and Mr. M. Takehara and Dr. M. Takahashi for advice on the study.

Supported by grants-in-aid of the Priority Area "Cancer" from the Ministry of Education, Culture, Sports, Science, and Technology, Japan, to T. Yamori (11177101); grants-in-aid for Scientific Research (B) from Japan Society for the Promotion of Science to T. Yamori (17390032); and a grant from National Institute of Biomedical Innovation, Japan, to T. Yamori (05-13).

Funding to pay the Open Access publication charges for this article was provided by the Japanese Foundation for Cancer Research.

Manuscript received September 16, 2005; revised January 23, 2006; accepted March 3, 2006.

THE JOURNAL OF BIOLOGICAL CHEMISTRY VOL. 281, NO. 25, pp. 17492–17500, June 23, 2006

Autotaxin Is Overexpressed in Glioblastoma Multiforme and Contributes to Cell Motility of Glioblastoma by Converting Lysophosphatidylcholine TO Lysophosphatidic Acid*

Received for publication, February 24, 2006 Published, JBC Papers in Press, April 19, 2006, DOI 10.1074/jbc.M601803200

Yasuhiro Kishi[‡], Shinichi Okudaira[‡], Masayuki Tanaka[‡], Kotaro Hama[‡], Dai Shida[§], Joji Kitayama[§], Takao Yamori[¶], Junken Aoki[‡1], Takamitsu Fujimaki[‖], and Hiroyuki Arai[‡]

From the [‡]Graduate School of Pharmaceutical Sciences, the University of Tokyo, 7-3-1 Hongo, Bunkyo-ku, Tokyo 113-0033, the [§]Graduate School of Medicine, the University of Tokyo, 7-3-1 Hongo, Bunkyo-ku, Tokyo 113-0033, the [¶]Division of Molecular Pharmacology, Cancer Chemotherapy Center, Japanese Foundation for Cancer Research, Toshima-ku, Tokyo 170-8455, and the [‖]Department of Neurosurgery, Teikyo University School of Medicine, 2-11-1, Kaga, Itabashi-ku, Tokyo 173-8605, Japan

Autotaxin (ATX) is a multifunctional phosphodiesterase originally isolated from melanoma cells as a potent cell motility-stimulating factor. ATX is identical to lysophospholipase D, which produces a bioactive phospholipid, lysophosphatidic acid (LPA), from lysophosphatidylcholine (LPC). Although enhanced expression of ATX in various tumor tissues has been repeatedly demonstrated, and thus, ATX is implicated in progression of tumor, the precise role of ATX expressed by tumor cells was unclear. In this study, we found that ATX is highly expressed in glioblastoma multiforme (GBM), the most malignant glioma due to its high infiltration into the normal brain parenchyma, but not in tissues from other brain tumors. In addition, LPA_1, an LPA receptor responsible for LPA-driven cell motility, is predominantly expressed in GBM. One of the glioblastomas that showed the highest ATX expression (SNB-78), as well as ATX-stable transfectants, showed LPA_1-dependent cell migration in response to LPA in both Boyden chamber and wound healing assays. Interestingly these ATX-expressing cells also showed chemotactic response to LPC. In addition, knockdown of the ATX level using small interfering RNA technique in SNB-78 cells suppressed their migratory response to LPC. These results suggest that the autocrine production of LPA by cancer cell-derived ATX and exogenously supplied LPC contribute to the invasiveness of cancer cells and that LPA_1, ATX, and LPC-producing enzymes are potential targets for cancer therapy, including GBM.

Autotaxin (ATX)[2] is a 125-kDa glycoprotein and a potent tumor cell motogen that was originally isolated from the conditioned medium of A2058 human melanoma cells as a cell motility-stimulating factor for melanoma cells (1). ATX was subsequently identified as a member of a family of ecto/exoenzymes referred to as nucleotide pyrophosphatases/phosphodiesterases (NPPs) (2, 3). The three cloned members of this family (PC-1/NPP1, ATX/NPP2, and B-10/NPP3) share a 47–55% amino acid sequence identity. PC-1/NPP1 and B-10/NPP3 hydrolyze 5′-phosphodiester bonds in nucleotides *in vitro*, whereas ATX/NPP2 shows only weak activity at hydrolyzing such bonds. ATX is synthesized as a type II membrane protein and is released from cells in a soluble form by an unknown mechanism (3, 4). Enhanced expression of ATX in Ras-transformed NIH3T3 cells greatly enhances their invasive, tumorigenic, and metastatic potentials (5). In addition, enhanced expression of ATX has been repeatedly demonstrated in various malignant tumor tissues including non-small cell lung cancer (6), breast cancer (7, 8), renal cell cancer (9), hepatocellular carcinoma (10, 11), and thyroid cancer (12), suggesting that ATX confers the tumorigenic and metastatic potentials of cancer cells. However, there is no direct evidence to show such a hypothesis so far.

The mechanism by which ATX exhibits its biological activity toward various cancer cells was unknown. An ATX point mutant that is deficient in 5′-nucleotide phosphodiesterase activity was found to abolish the cell motility-stimulating activity of ATX (13), indicating that the migratory response to ATX requires an intact catalytic site. Recently, we and others showed that ATX has lysophospholipase D (lysoPLD) activity, which catalyzes a reaction to produce a bioactive lysophospholipid, lysophosphatidic acid (LPA), from lysophosphatidylcholine (LPC) (14, 15). ATX has a significantly lower K_m for LPC than the K_m for the classical nucleotide substrate. Because LPA has long been defined as a cell motility-stimulating factor for various cell types including glioblastomas (16–18), ATX has been suggested to regulate motility by producing LPA through the G-protein-coupled receptor. Indeed, recent studies have shown that ATX stimulates the cell motility of various cancer cells *in vitro* through one of the LPA receptors, LPA_1 (19–22). Taking account of the fact that elevated ATX expression has been detected in various tumors (6–12), it is possible that certain cancer cells utilize the ATX-LPC-LPA-LPA_1 system for their motility. In these cells, a possible regulatory factor that remains to be characterized is LPC. LPC is always present in plasma. In human plasma, its concentration ranges from 100 to 300 μM. LPC is also detected in other biological fluids such as seminal fluids and cerebrospinal fluids and in tissues and various types of cells but at much lower concentrations than in plasma (23, 24).

Glioblastoma multiforme (GBM) is a highly malignant brain tumor. Removal of the tumor mass transiently improves the condition of the patient, but the ability of GBM cells to infiltrate normal brain tissue invariably almost always leads to tumor recurrence. Thus, most patients experience recurrence within 1 year (25), and less than 20% of the patients survive more than 2 years (26). GBM cells (glioblastomas) are highly motile and invade the normal brain parenchyma diffusely (27). Several factors responsible for their invasive phenotype have been

* The costs of publication of this article were defrayed in part by the payment of page charges. This article must therefore be hereby marked "*advertisement*" in accordance with 18 U.S.C. Section 1734 solely to indicate this fact.

[1] To whom correspondence should be addressed. Tel.: 81-3-5841-4723; Fax: 81-3-3818-3173; E-mail: jaoki@mol.f.u-tokyo.ac.jp.

[2] The abbreviations used are: ATX, autotaxin; GBM, glioblastoma multiforme; LPA, lysophosphatidic acid; LPC, lysophosphatidylcholine; lysoPLD, lysophospholipase D; RT, reverse transcription; BBB, blood-brain barrier; NPP, nucleotide pyrophosphatases/phosphodiesterases; CNS, central nervous system; siRNA, small interfering RNA; GAPDH, glyceraldehyde-3-phosphate dehydrogenase.

reported, such as certain extracellular matrix proteins including laminin, fibronectin, and/or collagen can promote glioma cell migration (28, 29). Secreted matrix metalloproteinases remodel the extracellular matrix, creating pathways more conducive to migration through normal brain tissue (30). Investigations of the factors that affect the motility of glioblastomas are of particular interest because an understanding of these factors is needed for valid GBM therapy. Because the blood-brain barrier (BBB) is disrupted in GBM tissue, some components in plasma might affect the cell motility of glioblastomas (31, 32). In this study, we examined the expression of ATX and LPA_1 in brain tumor tissues and various tumor cell lines and found that both ATX and LPA_1 are predominantly expressed in glioblastomas and GBM tissue. Using glioblastomas as a model system, we evaluated the effects of ATX, LPA_1, LPA, and LPC on the motility of the cells.

MATERIALS AND METHODS

Reagents—1-oleoyl-LPA (18:1) and 1-oleoyl-LPC (18:1) was purchased from Avanti Polar Lipids Inc. (Alabaster, AL). Ki16425 was kindly provided by Dr. Hideo Ohata (Kirin Brewery Co., Takasaki, Japan).

Cell Lines—All human tumor cell lines were maintained in RPMI 1640 (Sigma) supplemented with 2 mM glutamine, 1× penicillin/streptomycin, and 5% (v/v) heat-inactivated fetal bovine serum as described previously (33). The cell lines used in this study were NCl-H23 (lung), NCl-H226 (lung), NCl-H522 (lung), NCl-H460 (lung), A549 (lung), DMS273 (lung), DMS114 (lung), HCC-2998 (colon), HT-29 (colon), WiDr (colon), HCT-15 (colon), DLD1 (colon), SW480 (colon), LOVO (colon), CaRI (rectum), WiDr (colon), CaCo2 (colon), Colo320 (colon), Colo201 (colon), HCT-116 (colon), KM12 (colon), HT1080 (colon), RXF-631L (renal), ACHN (renal), OVCAR3 (ovary), OVCAR4 (ovary), OVCAR5 (ovary), OVCAR8 (ovary), SKOV-3 (ovary), U251 (CNS), SF295 (CNS), SF539 (CNS), SF268 (CNS), SNB75 (CNS), SNB78 (CNS), MKN45 (stomach), MKN28 (stomach), St4 (stomach), MKN1 (stomach), MKN7 (Stomach), MKN74 (stomach), KatoIII (stomach), MKN28 (stomach), MKN45 (stomach), MKN74 (stomach), MDA-MB231 (breast), HBC4(breast), BSY1 (breast), MCF7 (breast), DU145 (prostate), PC3 (prostate), HPC5 (others), A2058 (melanoma), and HeLa (uterine cervix). Mouse 203G glioma cells were maintained in RPMI 1640 supplemented with 2 mM glutamine, 1× penicillin/streptomycin, and 10% (v/v) heat-inactivated fetal bovine serum. This cell line was kindly provided by Dr. Koji Adachi (Nippon Medical School Tokyo, Japan).

Quantitative Real-time RT-PCR—From various cancer tissues and cancer cell lines, total RNA from cells was isolated using ISOGEN (Nippongene, Toyama, Japan) and reverse-transcribed using the SuperScript first-strand synthesis system for RT-PCR (Invitrogen). Oligonucleotide primers for PCR were designed using Primer Express Software (Applied Biosystems, Foster City, CA). The sequences of the oligonucleotides used in PCR were as follows: ATX (human), forward, 5′-GGGTGAAAGCTGGAACATTCTT-3′; ATX (human), reverse, 5′-GCCACCGCAATATGGAATTATAAG-3′; LPA_1 (human), forward, 5′-AATCGGGATACCATGATGAGTCTT-3′; LPA_1 (human), reverse, 5′-CCAGGAGTCCAGCAGATGATAAA-3′; LPA_2 (human), forward, 5′-CGCTCAGCCTGGTCAAGACT-3′; LPA_2 (human), reverse, 5′-TTGCAGGACTCACAGCCTAAAC-3′; LPA_3 (human), forward, 5′-AGGACACCCATGAAGCTAATGAA-3′; LPA_3 (human), reverse, 5′-GCCGTCGAGGAGCAGAAC-3′; LPA_4 (human), forward, 5′-CCTAGTCCTCAGTGGCGGTATT-3′; LPA_4 (human), reverse, 5′-CCTTCAAAGCAGGTGGTGGTT-3′; ATX (mouse), forward, 5′-GGAGAATCACACTGGGTAGATGATG-3′; ATX (mouse), reverse, 5′-ACGGAGGGCGGACAAAC-3′; LPA_1 (mouse), forward, 5′-GAGGAATCGGGACACCATGAT-3′; LPA_1 (mouse), reverse, 5′-ACATCCAGCAATAACAAGACCAATC-3′; LPA_2 (mouse), forward, 5′-GACCACACTCAGCCTAGTCAAGAC-3′; LPA_2 (mouse), reverse, 5′-CTTACAGTCCAGGCCATCCA-3′; LPA_3 (mouse), forward, 5′-GCTCCCATGAAGCTAATGAAGACA-3′; LPA_3 (mouse), reverse, 5′-AGGCCGTCCAGCAGCAGA-3′; LPA_4 (mouse), forward, 5′-CAGTGCCTCCCTGTTTGTCTTC-3′; LPA_4 (mouse), reverse, 5′-GAGAGGGCCAGGTTGGTGAT-3′; GAPDH (human/mouse), forward, 5′-GCCAAGGTCATCCATGACAACT-3′; GAPDH (human/mouse), reverse, 5′-GAGGGGCCATCCACAGTCTT.

PCR reactions were performed using an ABI Prism 7000 sequence detection system (Applied Biosystems). The transcript number of human GAPDH was quantified, and each sample was normalized on the basis of GAPDH content.

LysoPLD Assay—Samples were incubated with 2 mM LPC (14:0) in the presence of 100 mM Tris-HCl (pH 9.0), 500 mM NaCl, 5 mM $MgCl_2$, and 0.05% Triton X-100 during indicated hours at 37 °C. The liberated choline was detected by an enzymatic photometric method as described (14). Briefly, the liberated choline was oxidized by choline oxidase, and the hydrogen peroxide generated was quantified using horseradish peroxidase and TOOS reagent (*N*-ethyl-*N*-(2-hydroxy-3-sulfoproryl)-3-methylanikine, Dojin, Tokyo, Japan).

SDS-PAGE/Western Blotting—Both cells and cell media were used to test for ATX protein expression. Cells were homogenized in phosphate-buffered saline, and then the cell homogenates were separated into membrane and soluble fractions by centrifugation at 100,000 × *g* for 60 min. Protein samples were separated by SDS-PAGE and transferred to nitrocellulose membranes using the Bio-Rad protein transfer system. The membranes were blocked with 10 mM Tris-HCl (pH 7.5) containing 150 mM sodium chloride, 5% (w/v) skimmed milk, and 0.05% (v/v) Tween 20, incubated with anti-lysoPLD monoclonal antibody (3D1) (23), and then treated with anti-rat IgG-horseradish peroxidase. Proteins bound to the antibody were visualized with an enhanced chemiluminescence kit (ECL, Amersham Biosciences).

Isolation of Stable ATX Transfectant—The plasmid vector pCAGGS (kindly provided by Dr. Junichi Miyazaki (34)) was utilized to create rat ATX (ATX-t) tagged with the Myc epitope at the C terminus (pCAGGS-rATX-Myc). To establish stable transfectants, 203G glioma cells were transfected with pCAGGS-rATX-Myc using Lipofectamine Plus reagents (Invitrogen) as recommended by the manufacturer and were grown in RPMI 1640 containing 800 μg/ml G418 (Wako). Individual G418-resistant clones were isolated by limiting dilution and screened by immunocytochemistry using Myc antibody and by measuring the lysoPLD activities of the culture media.

Recombinant ATX Preparations—Rat ATX was expressed and partially purified using baculovirus system as described previously (14). The purified ATX was dialyzed in phosphate-buffered saline and used for cell motility assays.

Boyden Chamber Assay—Chemotaxis was assayed as described previously (21). In brief, polycarbonate filters with 8-μm pores (Neuro-Probe, Inc., Gaithersburg, MD) were coated with 0.001% fibronectin (Sigma). Cells (1×10^5 cells in 200 μl/well) were loaded into the upper chambers and incubated at 37 °C for 6 h to allow migration. Cell migration to the bottom of the filter was evaluated by measuring optical density at 590 nm. For Ki16425 treatment, cells were preincubated with 1 μM Ki16425 for 30 min.

Wound Healing Assay—Cells were plated in cell culture plates (12-well) using cell growth media containing fetal bovine serum. After the cells had reached semiconfluence, fetal bovine serum was removed from the media and replaced with serum-free media. A plastic pipette tip was drawn across the center of the plate to produce a clean wound area 24 h

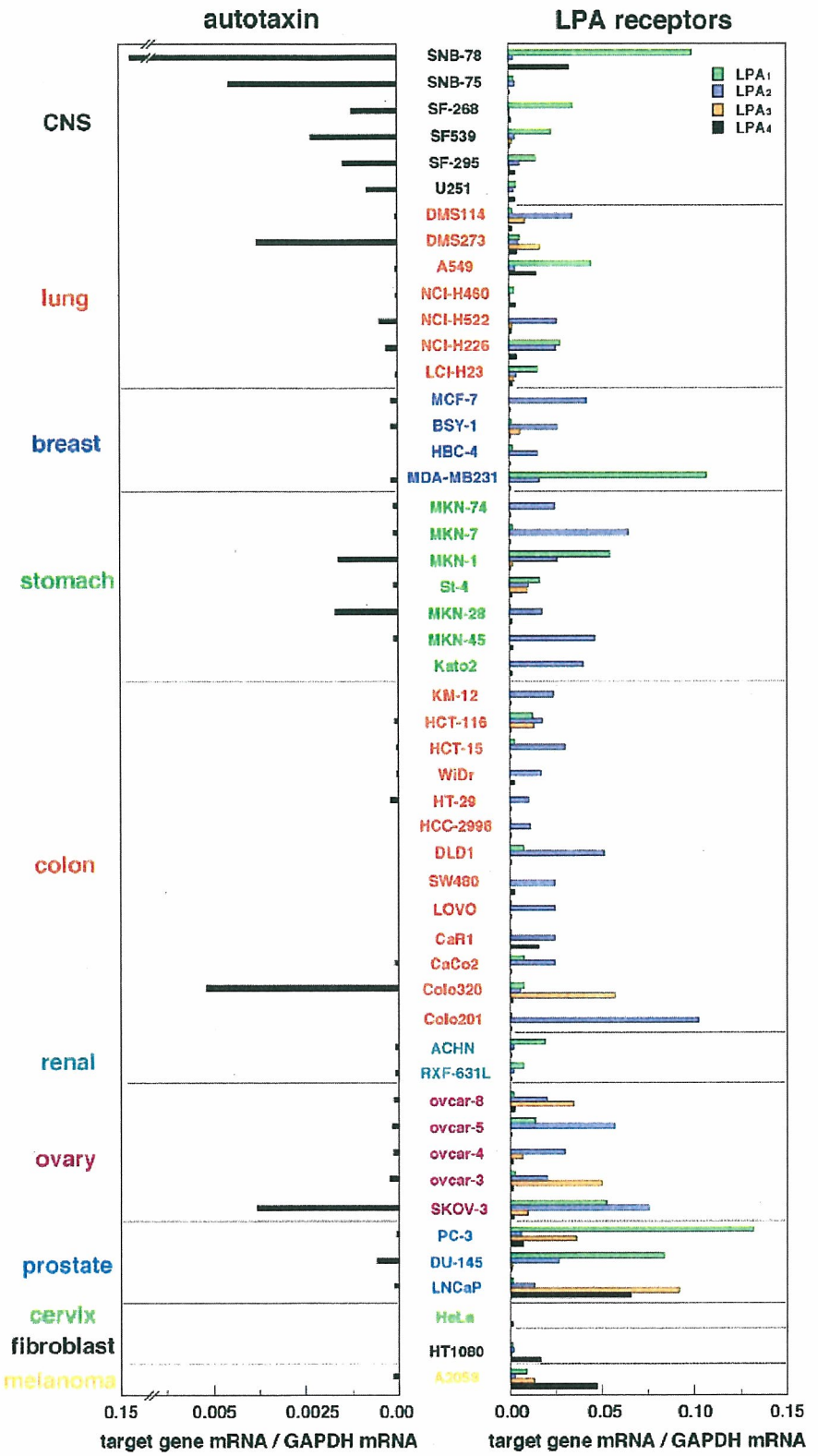

FIGURE 1. **Expression profiles of ATX and LPA receptors in tumor cell lines.** A quantitative RT-PCR analysis of ATX (*left*) and LPA receptors (LPA_1, LPA_2, LPA_3, and LPA_4, *right*) in 50 tumor cell lines from various origins (CNS, lung, breast, stomach, colon, kidney, ovary, prostate, cervix, fibroblast, and melanoma) was performed. Values are expressed relative to the expression of GAPDH mRNA.

after serum depletion. Medium was then replaced with serum-free medium containing different concentrations of 1-oleoyl-LPA, 1-oleoyl-LPC, Ki16425 (1 μM) and lysoPLD. After the cells were cultured for 12, 24, or 36 h, cell movement into the wound area was examined. The migration distances between the leading edge of the migrating cells and the edge of the wound were compared.

Quantification of LPC—LPC concentration in cell culture supernatant was determined as described previously (35). Briefly, cells were